Università degli Studi di Palermo

AREA QUALITÀ, PROGRAMMAZIONE E SUPPORTO STRATEGICO
SETTORE STRATEGIA PER LA RICERCA
U. O. DOTTORATI

D067 - Technologies and Sciences for Human Health
Dipartimento di Scienze e Tecnologie Biologiche Chimiche e Farmaceutiche (STEBICEF)
SSD: BIO/11

"Analysis of the effects of innovative radiotherapy treatments in zebrafish"

LA DOTTORANDA
Gaia Pucci

IL COORDINATORE
Prof. Vincenzo Cavalieri

IL TUTOR
Prof. Vincenzo Cavalieri

CO TUTOR
Dott.ssa Giusi Irma Forte

CICLO XXXV
ANNO 2023

INDEX

INTRODUCTION

1. Radiotherapy

Conventional radiotherapy (RT) protocols are based on the administration of photon beams in the form of low *Linear Energy Transfer* (LET) radiation (X-rays, γ-rays), which deposit a relatively small amount of energy on the target and disperses it further to the surrounding healthy tissue due to *scattering phenomena*, differently from high LET radiations (protons, neutrons), which produce higher biological damage on the target with minimal dispersion on the close non irradiated tissues.

The so-called *Linear and No-Threshold* (LNT) model has been recognized for half a century as the methodological basis to predict stochastic and long-term biological damage caused by *Ionizing Radiation* (IR). According to the theory of "stochastic breakage" of one or both the DNA double helix strands, high LET radiation generally induces "direct" damages on both DNA strands (*Double Strand Breaks*, DSBs) and macromolecules, proportional to the dose and exposure duration, often irreparable, and promoting cell killing. On the other hand, low LET radiations cause damage resulting from indirect interaction with the matter, where the damage on DNA and other macromolecules is prevalently due to the release of free radicals and *Reactive Oxygen Species* (ROS), produced by water radiolysis in cell cytoplasm (*Wakeford, 2008*). In this second case, *Single Strand Breaks* (SSBs) are prevalent and easily repairable, resulting in not permanent damages. Thus, low-LET radiation is more dependent on the so called "oxygen effect", as free radicals and oxidized macromolecules are produced, contributing to the damaging of biological structures (**Fig. 1**).

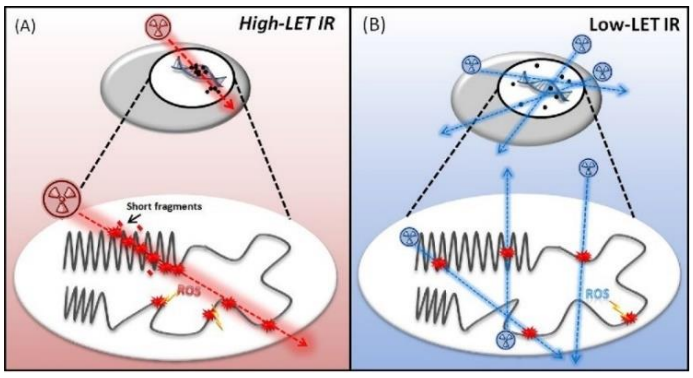

Fig. 1 *High-LET versus low-LET IR induced DNA damage. (A): High-LET IR, respect to low-LET IR (B), has both high energy and high mass, producing densely spaced damage through chromatin, across a short distance (Moore et al., 2014. DOI: 10.1016/j.dnarep.2014.01.014).*

Nowadays *Proton Therapy* (PT) represents a valid alternative to photon RT for the treatment of specific types of cancer. The therapeutic use of proton beams (and of any charged particles) is primarily motivated by their inverted depth-dose profile, so that unlike photons, these particles release a smaller amount of energy in the initial phase of penetration into the patient's body, concentrating the maximum release of energy at the end of their path, in the so-called Bragg peak, i.e. on the tumor target. So, protons are characterized by more effective and selective delivery of energy to the target, generating limited damage in the surrounding healthy tissues. Considering how the dose should be conformed to the entire target volume and how it should be homogeneously distributed, the peak is enlarged to obtain a *Spread-Out Bragg Peak* (SOBP), which is obtained by overlapping several Bragg peaks relating to single beams of different energies and intensities (different LETs but constant dose). Protons and charged particles showed an enhanced *Relative Biological Effectiveness* (RBE) in cell killing, and this is related to the increased LET compared to X-rays in the region close to the Bragg peak, resulting in the induction of enhanced, unrepairable biological damage (*Paganetti et al., 2002; Goodhead, 2006*) (**Fig. 2**). Consequently, charged particles are often defined as densely ionizing radiation, in contrast to photons, being considered sparsely ionizing radiation.

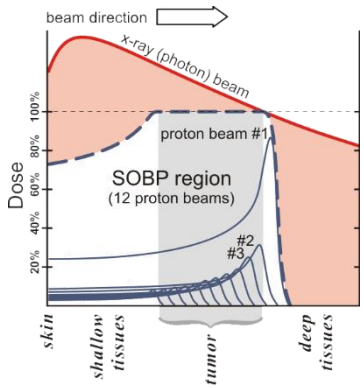

Fig. 2 *Dose profile of a typical hadrontherapy treatment as SOBP, i.e. sum of multiple Bragg peaks (dashed blue line). For comparison, the dose-depth profile for an X-ray beam is shown in red. The pink area represents the excess dose for RT over hadrontherapy, which*

can cause further damage to healthy tissue (AISF, Feb 1, 2018. L'adroterapia contro i tumori. FOOT: il nuovo esperimento dell'INFN. Neri F, Alma Mater Studiorum - Università di Bologna. https://ai-sf.it/sistemidiriferimento/2018/02/01/FOOT-BO/).

The increased effectiveness of charged particles compared to photons is quantified by the RBE, defined as the *ratio* between photon and charged particle doses necessary to obtain the same biological effect (**Fig. 3**), that numerous studies have experimentally calculated close to 1.1 for protons and 3 for carbon ions (*Tubin et al., 2023*). In a clinical context, RBE represents a key parameter to compare hadrotherapy treatment plans to X-rays for prescribed doses.

However, the RBE is a complex quantity, depending on physical parameters (i.e. particle type, dose, LET) as well as on biological ones (i.e. tissue type, cell cycle phase, oxygenation level, end point) (*Paganetti, 2014; Tommasino et al., 2014*).

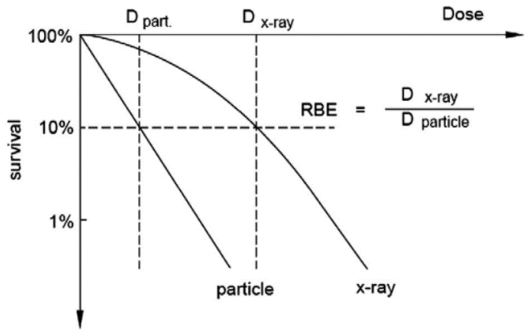

Fig. 3 *Definition of RBE, illustrated for cell survival curves. (Desouky and Zhou, 2016. DOI: 10.1016/j.jtusci.2015.02.014).*

1.1 Radiation-induced normal tissue toxicity

Concerning the dose-dependence of biological effects, in 1973 it was developed the *Linear Quadratic* (LQ) model, till now considered a key tool to describe the relationship between radiation dose and survival of living cells.

However, the evidence of recent years makes these "classic" models increasingly less acceptable and to be surpassed, considering that exposure to low doses of IR seems to have long-term carcinogenic effects, in exposed individuals and in subsequent generations. This is due to the fact that survived cells to low-dose exposure have been shown to accumulate damage, evident

in their progeny and in not directly irradiated cells, such as surrounding normal tissue. This is related to the exchange of molecular signals (oxygen radicals, nitrogen radicals and cytokines) and complex tissue reactions between near or distant cells (*Burgio et al., 2018*). This fact was reported for the first time in the 1950s but demonstrated only in the early 1990s, under the name of *bystander effect* (*Tang et al., 2023*). In particular, cells located closely to the irradiation site respond individually and collectively as part of a large, interconnected, *web*, with signals that could alter the dynamic equilibrium between proliferation, apoptosis, quiescence, or differentiation (*Marín et al., 2015*). Therefore, mutations, micronuclei formation, chromosome breaks and sister chromatid exchanges, as well as low-grade systemic inflammatory responses, can arise in neighbouring cells not directly affected by radiation (*Banaz-Yasar et al., 2007*). Depending on the nature of the chromosomal change, the mutation might lead to cell death or induce cancer formation, if the mutation happens to either turn on an oncogene or turn off a tumor suppressor gene (*Hall and Giaccia, 2006*). In addition, the possibility that the damaging effects suffered by cells (and DNA) could slowly accumulate over the time and that cumulative damages effect could occur even after months or years, led the researchers to think that it made no sense to propose a linear link between the initial dose and the biological damage (*Lyng et al., 1996*), especially considering that minimal doses of radiation (as 2 mGy) were often sufficient to produce these long-term effects (*Mothersill et al, 2003*).

Rapid proliferating cancer cells are usually more sensitive to radiation than normal cells, so that they can usually repair themselves at a faster rate. So, the purpose of therapeutic plans is to inhibit, as much as possible, cancer cell multiplication, possibly leading to cell death, while minimizing dosage absorption in normal tissue, to prevent adverse effects and toxicity (*Baskar et al., 2014*).

Thus, normal tissue response to IR has been a major subject of study since the discovery of X-rays at the end of the 19th century (*McBride et al., 2020*), and it remains the dose-limiting factor to achieve full tumor control in clinical RT. During RT, about 90% of patients experience acute skin toxicities, related to apoptosis and necrosis even weeks after irradiation (*Najafi et al., 2018*). Indeed, exposure of normal tissue to radiation can cause both acute and

chronic toxicities, with chronic symptoms or severe organ dysfunction that can produce a decrease in quality of life (*Citrin et al., 2010*), leading to the inability to administer the intended therapy.

In particular, conventional RT produces high incidence of dermatitis, pneumonitis, cataract genesis, neurocognitive impairment, myelosuppression, secondary malignancies, and mucositis/enteritis (*Yorke et al., 2002*). The skin irradiation inhibits connective tissue proliferation, formation and maturation of granulation tissue, collagen transcription and secretion and neovascularization, all of them fundamental to wound healing (*Bernstein et al., 1993; Gu et al., 1998*).

Radiation-induced damages on normal tissue may vary depending on the volume of irradiated organ, the cell proliferation rate or intracellular and microenvironmental factors, the type of radiation, the dose delivered, its fractionation, the administration of radiation modifiers, and individual radiosensitivity (*Blank et al., 1997; Meng et al., 1998*). In addition, tissue composition, and in particular its turnover time or the plasticity in response to injury, clinically impacts the fractionated radiation schedules (*Wabik and Jones, 2015*). Particularly, tissues with rapid turnover are defined as "early responder", and they have stem/progenitor populations which respond and regenerate rapidly, so they are more radiosensitive and exhibit a lesser effect of dose fractionation. Instead, slow-turnover tissues are "late responder" to IR, having less dependence on stem/progenitor cells for regeneration, relying more on the proliferation and reprogramming of more mature cells (*Boerma et al., 2022*). They are more radioresistant and require fractionated protocols for depositing the dose necessary to obtain a good probability of tumor control. Despite improved treatment modalities and advanced RT technologies has made RT safer than before, it is still important to broaden the therapeutic window between normal tissue damage and tumor suppression (*Groves et al., 1999*). Image guided RT treatments have made substantial progress in reducing the exposure of normal tissues to the prescribed dose. However, it is still necessary to find alternative and personalized treatment methods that can lead to more successful RT protocols (*Citrin et al., 2017*), pursuing two strategies of clinical importance: radiosensitization of tumor cells and radioprotection of normal ones (*Vasiliki et al., 2022*).

Several studies have been carried out and several possible alternatives were evaluated to outline potential therapeutic options in this context.

1.2 The therapeutic window

Over the past four decades, research has enhanced the understanding of the pathophysiological, cellular, and molecular complex processes governing normal tissue toxicity, going deeper the involvement of the crosstalk between the various cells of the treated tissue (*Montay-Gruel et al., 2019*). The RT therapeutic window for each tissue is described by the difference between the *Tumor Control Probability* (TCP) and the *Normal Tissue Complication Probability* (NTCP), which are described by sigmoid curves (**Fig. 4**) (*Warkentin et al., 2004*).

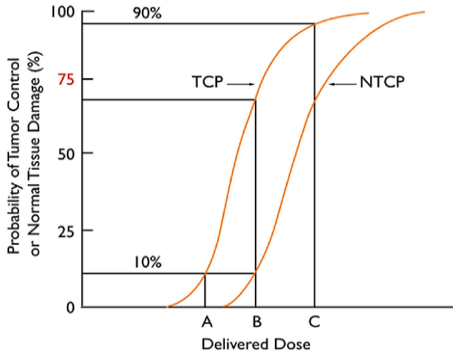

Fig. 4 *Descriptive curves of TCP and NTCP equations (Warkentin et al., 2014. DOI: 10.1120/jacmp.v5i1.1970).*

Several physical factors can modulate this window; however, by increasing the dose or the radiation volume, both probabilities tend to increase. Moreover, recent technological advances in radiation delivery have been made to maximize the dose delivery on the tumor, saving the surrounding healthy tissues, such as *Intensity-Modulated RT* (IMRT), *Image-Guided RT* (IGRT), or other non-conventional RT treatments using hadrotherapy with protons or carbon ions (*Forte et al., 2017*).

On the other hand, several other genetic and biologic features affect the tissues radiosensitivity, such as the tumor location or its cell repopulation rate. Other approaches used to modulate the treatment tolerance include the RT treatment schedule modification, playing on the dose fractionation, which is the time of total dose administration. The dose fractionation increases the

tolerability of normal tissues and, at the same time, reduces the radioprotective effects of hypoxia on the tumor; i.e. 2 Gy/day for a total dose of 60 Gy is the standard conventional protocol used for *Breast Cancer* (BC) RT treatment, even if several clinical trials are testing ipo- or iper-fractionated RT treatment dedicated to the various tumor types (*Savoca et al., 2020*). Finally, the therapeutic window can be modified by combining RT with other treatment modalities such as chemotherapy, or the use of radiosensitizers and radioprotectors molecules, the last ones specifically increasing the tumor radiation response while decreasing toxicity on healthy tissue, respectively (*Prasanna et al., 2012*). Since the normal tissue complications derived from the RT treatment cannot be completely avoided, research on healthy tissue tolerance is currently focusing on the possibility of applying innovative combined RT protocols, based on the administration of low-toxic and very effective compounds, with a radioprotective role.

1.3 Radioprotectors

The use of a wide range of pharmaceutical compounds, many of them chemotherapeutic, seems to enhance the desired effects on the irradiated tumor mass, although most of them are toxic at therapeutically effective concentrations, and very few substances have passed clinical trials and are currently used as adjuvants (*Lin et al., 2020*). Therefore, optimizing drug *ratios* and schedules can provide an opportunity to improve drug combination activity and reduce dosages to attenuate toxicity (*Wu et al., 2017*).

Radiation modifiers could also be represented by natural compounds, that can easily be recovered and are less expensive when compared to synthesized drugs. Their use minimizes collateral effects ameliorating the poor quality of life of oncological patients (*Calvaruso et al., 2019*). Bio-active compounds isolated from natural sources (as crude extracts of various medicinal plants, purified fractions, and herbal preparations) and enriched with antioxidants, usually called “scavengers”, possess unique immune-modulating properties, thus providing a double benefit over synthetic radioprotectors. These compounds could protect cells by scavenging free radicals, thus preventing their interaction with biochemical molecules (*Murray et al., 1998*). In this way, redox homeostasis can be maintained (**Fig. 5**).

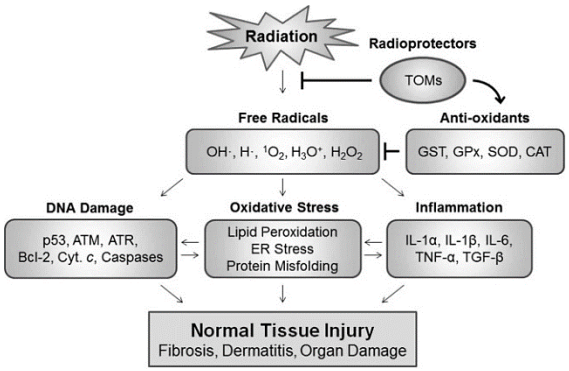

Fig. 5 *Mechanism related to the radioprotective effects of some compounds. Radiation induces formation of free radicals in the cells, which subsequently stimulates DNA damage response, oxidative stress response and inflammation. These events act as major causes for normal tissue injuries including fibrosis, skin dermatitis and organ damage (Kim et al., 2017. DOI: 10.3892/ol.2017.6042).*

Interestingly, some phytochemical foods exhibit both antioxidant and pro-oxidant activities, depending on their concentration and cellular microenvironment. Indeed, there is evidence that concurrent administration of some dietary phytochemicals enhances the efficacy of certain cancer treatments by increasing intracellular ROS accumulation while protecting the surrounding healthy tissue at the same time (*Wasundara Fernandoa et al., 2019*). It has been shown that a biologically active molecule, such as a phytochemical, could induce a positive response (*low dose stimulation*) when given at low concentration, for adaptation or protection from stress factors, while it results in a toxic response, when it is present at a higher concentration (*high dose inhibition*). This biological phenomenon, called *hormesis*, explains this biphasic dose-response behaviour of a natural substance, pharmaceutical drug, or toxin (*Calabrese et al., 2010*).

Among these compounds, Curcumin [(1E,6E)-1,7-bis (4-hydroxy- 3-methoxyphenyl) -1,6- heptadiene-3,5-dione)] is a natural substance that has been seen to act with the dual role of radioprotector and radiosensitizer in association with IR, by *in vitro* studies (*Minafra et al., 2019*). Curcumin can sensitize cancer cells to irradiation and could play a key interesting role in radiosensitivity/radioresistance and radioprotection cell balance (*Chendil et al., 2004*), through mechanisms that could be summarized into three approaches: direct enhancement of the tumoricidal effect (sensitizing cancer cells to be more responsive to RT), reversing radioresistance (reducing the

pro-survival response mechanisms of cancer cells), and alleviating toxicity induced by RT protocol on normal tissues.

2. Curcumin

Curcumin has been explored *in vitro* and in animal models as potential option to reduce the stress pathways associated with radiation response and to improve wound healing in radiation-damaged skin, respectively (*Zoi et al., 2022*).

Turmeric (*Curcuma longa Linn.*) is a member of the *Zingiberaceae* family, and it is cultivated in tropical and subtropical regions around the world, although it originates from India, Southeast Asia, and Indonesia. Its pharmacological activity has been attributed mainly to curcuminoids, which are curcumin and two related compounds: the demethoxy curcumin and the bisdemethoxycurcumin (*Paramasivam et al., 2009*). Curcuminoids are phenolic compounds commonly used as spice, pigment, or additive in several foods, also utilized as therapeutic agents, due to their key roles in the control of inflammation and oxidative stress in many conditions. Their use in indigenous medicine for the treatment of sprain and inflammatory diseases has been known for centuries, under the name of turmeric and derived from the powder form of rhizome. They appear as crystalline compounds, with a bright orange-yellow colour. Between them, curcumin makes up about 90% of the curcuminoids present in turmeric, and it is a polyphenol with the molecular formula $C_{21}H_{20}O_6$ (**Fig. 6**).

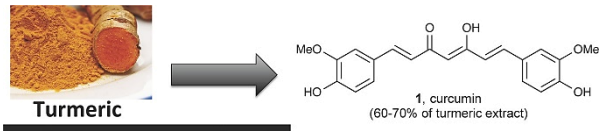

Constituent	Composition (w/w)
Curcuminoids	1–6%
Volatile (essential) oils	3–7%
Fiber	2–7%
Mineral matter	3–7%
Protein	6–8%
Fat	5–10%
Moisture	6–13%
Carbohydrates	60–70%

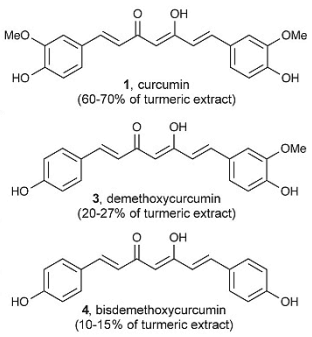

Fig. 6 *Major phytoconstituents of extracts of Curcuma longa. Compounds 1, 3, and 4, often grouped together as "curcuminoids", generally make up approximately 1–6% of turmeric by weight. Of a curcuminoid extract, 1 makes up 60–70% by weight, while 3 (20–27%) and 4*

(10–15%) are minor components (Nelson et al., 2017. DOI: 10.1021/acs.jmedchem.6b00975).

Curcumin, extracted in a pure crystalline form for the first time in 1870 (*Goel et al., 2008*) but characterized only later, in 1910 (*Ruby et al., 1995*), is widely reported to have remarkable medicinal and antineoplastic properties. Its multiple pleiotropic effects are related to the ability to interact and regulate multiple molecular targets such as *Transcription Factors* (TFs), growth factors, kinases, pro-inflammatory cytokines, adhesion molecules, etc. Various studies suggest that this compound has extensive biological activity as antioxidant, neuroprotective, antitumor, anti-inflammatory and radioprotective (*Amalraj et al., 2016*). These properties are attributed to the key elements in its structure (*Aggarwal et al., 2014*), with two phenyl rings substituted with hydroxyl and methoxyl groups, connected via a seven carbon keto-enol linker (C7) (*Chen et al., 2006*). However, the curcumin uses are limited due to its low water solubility at acidic and neutral pH, whereas it is soluble in methanol, ethanol, *Dimethyl Sulfoxide* (DMSO), and acetone. After oral administration, curcumin is metabolized by reduction and conjugation, producing metabolites whose biological activities are strongly reduced compared to that of curcumin. Its low absorption, bioavailability and high metabolism rate make it an unstable, reactive, and unavailable compound with poor *pharmacokinetic/pharmacodynamic* (PK/PD) properties (*Nelson et al., 2017*). So, to overcome these obstacles and improve its activity, several structural modifications have been suggested to increase bioavailability or stability (*Murgia et al., 2020*). Among the new strategies to increase its cellular absorption, the best way would seem to be the curcumin trapping into a nanoparticle carrier (*Chen et al., 2020*), to realize a molecule with lower chemical difficulties and higher potential for future biomedical applications.

2.1 Curcumin as radioprotector

Since one of the most prominent cancer pathogenic factors is of inflammatory nature, it seems clear that the curcumin anti-inflammatory powerful effects could down regulate inflammation and ROS production in surrounding normal tissue, as well as the RT induced fibrosis (**Fig. 7**).

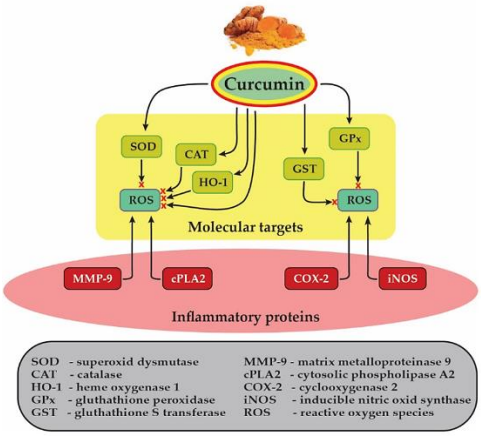

Fig. 7 *The molecular targets, anti-inflammatory and antioxidant mechanisms of curcumin on the normal cells. (Salehi et al., 2020. DOI:10.3390/jcm9020430).*

Previous *in vitro* results suggested that this protective mechanism depends on TGFβ decrease and, mainly, on the NF-kB inhibition (*Bravatà et al., 2013*), as well as on mitochondrial GSH increase or phase II detoxifying enzyme genes activation through Nrf2 signalling pathway, inducing a cellular protection against oxidative injury (*Milad et al., 2020*).

Minafra et al. (2019) evaluated the intracellular ROS levels in the MCF10A, MDA-MB-231 and MCF7 cell lines 24 hours after treatments with 2 Gy vs 2 Gy + Curcumin-SLN (*Solid Lipid Nanoparticle*), with the DCFH-DA (*2,7-Dichlorofluoroscin Diacetate*) molecular probe. The treatment with curcumin in combination with IR was able to lower the cellular ROS level respect to that observed in samples treated with only IR. In addition, the metabolomics analysis confirmed that the administration of Curcumin-SNL was able to play a protective role against oxidative stress induced by IR.

Srinivasan et al. (2008) also evaluated the radioprotective effect of Curcumin (CUR) analog [(bis-1,7-(2-hydrocyphenyl)-hepta-1,6-diene-3,5-dione)] on γ-radiation induced toxicity in primary cultures of isolated rat hepatocytes. Pre-treatment with different concentrations of CUR-analog showed a significant decrease in the levels of thiobarbituric acid reactive substances, inhibition on peroxidation of membrane lipids and free radicals-induced DNA strand break formation.

It has been revealed that chromosomal aberrations are formed by interaction of free radicals with DNA, which can cause cytogenetic damage. The radiation-induced cytogenetic damage in bone marrow of mice after curcumin

administration was evaluated by micronucleus test, and it has been demonstrated that a significant decline in the number of MnPCE occurred when curcumin was orally administrated to mice as pre-IR treatment (*Abraham et al., 1993*).

Although the low efficacy in several disease models as well as the toxic effects arising from certain testing conditions, a preclinical study also evaluated the effects on cutaneous toxicity induced by exposure to IR alone or in combination with curcumin. Intragastric and intraperitoneally administration of curcumin was given to C3H/HeN mice 5 days before or after RT (50 Gy, single dose, in the posterior leg of each mouse). Skin damage was assessed at 15–21 and 90 days post IR, to evaluate the acute and chronic cutaneous toxicity, respectively. The results showed that curcumin, for both the administration timepoints, markedly reduced acute and chronic cutaneous toxicity, significantly decreasing the expression of inflammatory IL-1, IL-6, IL-18, IL-1Ra and fibrogenic (TGF-β) cytokines in irradiated skin and muscles (*Bravatà et al., 2013*).

Similarly, as described by another research group in 2020, in 40 rats exposed to curcumin for 4 consecutive days - 1 day pre- and 3 days after-IR -, the levels of antioxidant enzymes as *Catalase* (CAT), *Superoxide Dismutase* (SOD), and *Malondialdehyde* (MDA) compound, were found considerably elevated compared to the only irradiated rats, suggesting that curcumin stimulates an increase in the antioxidant response (*Shabeeb et al., 2020*).

These are just a few examples, among a large number of *in vitro* and preclinical evidence, which describe and confirm that curcumin could play a radioprotective role in normal cells. However, considering this field relevance, this compound needs to be stringently analysed in other different models and conditions of radiation injury.

3. Zebrafish model in research

The zebrafish is a validated vertebrate model for disease, drug screening, target identification and pharmacology (*Calum and Randall, 2015*).

Although cell cultures will remain a cornerstone of research, mainly for their ease of use, they do not allow multidirectional research. So, animal models are essential for the study of physiological and pathological *phenomena*, such

as the carcinogenesis stages (*Völkel et al., 2018; Kwiatkowska et al., 2022*). The mouse models, to date, are the most used. However, they have several negative points, including the high costs of maintenance and research, the long waiting times for the offspring and their limited number, as well as the fact that the rodents are hairy, which makes it impossible to visualize any processes in real-time; furthermore, not to be underestimated, rodents carry out their physiological activity at night, clearly detaching themselves from humans (*Takashi et al., 2011*).

The spreading of zebrafish research field came in the early 1990s with the so-called "Big Screen", undertaken by the Nobel Prize winner Christiane Nusslein-Volhard at Max Plank Institute in Tubingen and her student Wolfgang Driver at Massachusetts General Hospital (*Meyer et al., 2018*). This ambitious initiative was a genome-wide screening on zebrafish, which started in 2001 and led to the categorization and description of thousands of zebrafish mutant lines. In 2013, the just published complete DNA sequence showed approximately 26.000 protein-coding genes, over 1.4 billion base pairs on 25 pairs of chromosomes. Comparison to the human genome, also revealed 70% of homology and 82% of orthologous human disease-related genes (*Howe et al., 2013*).

Considering this, the use of zebrafish is suitable for studying a variety of different situations, such as genetics, cell biology, toxicology, and embryology (*Arjmand et al., 2020*). So, the small freshwater cyprinid fills a scientific *niche* between *in vitro* models and higher organisms (*Horzman et al., 2018*).

Concerning toxicity assays, *Sipes et al. (2011)* reviewed the concordance of 55–100% between zebrafish and mammalian models in evaluating chemicals with toxic effects (*Brannen et al., 2010; Padilla et al., 2011; Selderslaghs et al., 2009*). The percent concordance across the mammalian species suggests that the response of zebrafish is on par with mammalian toxicity models and supports the utility of the zebrafish model in toxicology research, and for identifying clinically relevant drug targets and compounds interfering with tumor progression. Its main advantages are a fast response time, cost efficiency for drug testing, efficient manipulation of the host microenvironment by genetic tools, suitability for small molecule drug

screening, easy maintenance, transparency for easy observation, high fecundity, and rapid generation time. However, all these specifications will be described in the next paragraph (**Fig. 8**).

The key point is that zebrafish model is a good alternative *in vivo* model to mammals for robust testing of drug candidates for any therapy, as well as to test and validate any protocols (*Somasagara et al., 2022*).

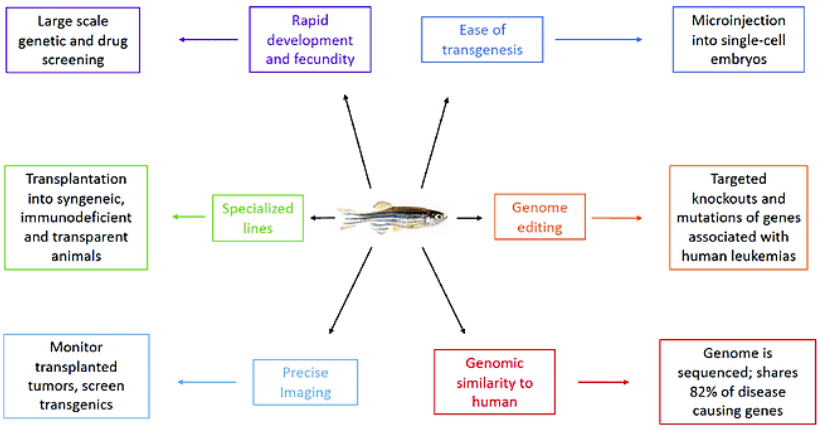

Fig. 8 *Advantages of the zebrafish model for the research (Baeten and de Jong, 2018. DOI: 10.3389/fcell.2018.00115).*

3.1 Zebrafish in cancer research and radiotherapy

Furthermore, in the *era* of personalized treatments, zebrafish model could be a useful screening tool for studying the effects of different radiation qualities and modifiers in a complex organism (*Steel, 1993*). As described by the *PubMed timeline* resulted from the *search query* "zebrafish and radiotherapy", the interest in this scientific area has been steadily growing from 2002 until 2022 (1 *vs* 24 papers). Most of the research has focused on the comparative study of the effects induced by different types of beams, while increasing literature is also available on the evaluation of compounds as possible radiomodifiers for the combined RT (*Pucci et al., 2021*).

Several positive properties of this model make it highly applicable in the radiobiology field of research.

First, these fish are quite small (adults are about 2–3 cm long), of ready abundance and accessibility and they can be easily maintained in the laboratory without excessive costs. The high fertility rate, combined with short generation time and large number of offspring, reduces the time to

produce experimental replicates, thereby increasing their potential for statistical validity (*Pucci et al., 2021*).

Zebrafish has wide tolerance regarding its maintenance (*Daroczi et al., 2006*) and transportation, and considering that embryos do not require sterile condition, they are better suited for radiobiological studies at non-hospital research radiation sources.

Embryos development is *ex utero* and extremely rapid*:* all major organs and tissues - for the majority comparable in position and function to those of humans - are fully developed within 48 *hours post fertilization* (hpf) (*Chang and Hwang, 2011*), and this allows to carry out a very detailed post-treatment phenotypic analysis in a very small time window. In addition, embryos are completely transparent until 72 hpf, and this makes it possible to study their development and possible alterations in real-time, as well as the possibility to make *xenograft* tumor model of patient-derived primary cells or immortalized laboratory cell lines by microinjection at early stages (*zebrafish patient-derived xenograft*, zPDX) (*Chen et al., 2021*).

There are different methods for establishing a cancer model in zebrafish:

1) the carcinogenic treatment, by inducing different gene mutations or activating signalling pathways through the use of chemicals;
2) the transplantation of mammalian tumor cells, that is possible because the immature adaptive immune system of zebrafish embryos accepts the transplantation of human cancer cells with no need for immunosuppression (*Trede et al., 2004*);
3) transgenic technology, leading to the formation of specific tumor types by the reverse genetic approaches, to create a loss-of-function phenotype or to transfer genes found mutated in human cancer patients into the fish.

In each of these cases, these models can also provide valuable information on the molecular biology of tumours and personalized RT protocols for cancer patients (*Costa et al., 2020*).

During organogenesis, zebrafish embryos are freely permeable to water, electrolytes, and a range of cryoprotectants such as methanol, DMSO, ethylene glycol and propane-1,2-diol, some drugs, small molecules as well as peptides and dyes, so providing easy access for compounds administration,

that can be directly administered into the fish water, and vital dye staining (*Rawson et al., 2000; Kari et al., 2007*).

As can be imagined, embryogenesis is the most radiosensitive stage of the vertebrate life cycle due to rapid cell division (*Hwang et al., 2007*), and the aqueous environment in which the embryos develop promotes homogeneous distribution of the irradiation dose.

With an irradiation size of about 1 mm, between the surface cell layer and subcutaneous tumours or normal tissue organs, zebrafish embryos could be used to study the RBE parameter and for detailed investigations on the RBE–LET relationship, both for low- and high-LET radiation types, in association or not with radiomodifying compounds (*Pucci et al., 2021*).

Last but not least there are, as the radiobiology literature has already widely described, materials and methods suitable to irradiate zebrafish embryos, such as configuration set up of irradiation in suitable supports, by the description of beam simulation studies, as well as methods to analyze IR induced toxicity, through the qualitative identification of specific embryos alterations and their quantification using dedicated scoring scales (*Szabó et al., 2016; Szabó et al., 2018; Brunner et al., 2020*).

Despite the aforementioned benefits, it must be remembered that the zebrafish model has certain disadvantages. Specifically, it is missing of some equivalent mammalian organs, such as lung, prostate, skin, and breasts gland. Therefore, the use of the zebrafish system, widely validated for some pathological conditions, is not able to replace classic mammalian testing systems; so, it can certainly precede and complement them as a first step towards the discovery of innovative and personalized treatments. However, it follows that zebrafish embryos provide a rapid and simple system to screen novel agents to be used as radiomodifiers.

AIMS

Pre-clinical models are a fundamental component in the field of radiobiological research. In this thesis we describe the use of zebrafish (*Danio rerio*) embryos as a model for the *in vivo* characterization of the biological effects induced by different types of beams, such as photons or protons, upon variation of specific radiobiological parameters, in combination or not with curcumin as a radiomodifying agent. The main purpose was to test the effects of curcumin as radioprotector for normal tissues in a sensitive model such as zebrafish embryos, in order to suggest this natural compound administration in association with IR, to improve the radiobiological performance of RT treatment, rendering it more effective and less toxic.

Starting from what has already been described in the literature, we defined the experimental setup for a reproducible irradiation of this model, both with photon or proton beams, which describe different penetration profiles into the tissues and require dedicated simulations. Furthermore, we defined the multiparametric embryo-larval workflow to analyze the toxic effects related to curcumin treatment. The aim of a combined treatment with RT is to reach greater biological effectiveness with the lowest compound concentration and dose irradiation, to maximize the RT efficacy and/or to reduce the toxic effect on the surrounding healthy tissues. Thus, focusing our studies on healthy tissue reactions, we firstly determined the *in vivo* specific thresholds of non-lethal and non-toxic curcumin concentrations to be used for the subsequent combined treatment. Afterwards, the embryos were subjected to increasing doses of IR in order to define lethality ranges and typical development alterations associated with the dose escalation. Finally, we determined the *in vivo* role of curcumin as a radiation modifying agent, describing changes in development alterations in response to combinations of curcumin, at two interesting concentrations, and increasing doses of IR. Thus, single or combined treatments of significant interest were explored at a molecular level.

Overall, our attention was focused on the curcumin pre-treatment ability to protect the zebrafish embryos from morphological and physiological

alterations or death, due to the IR treatment, identifying the molecular mechanism underlying these biological effects.

MATERIALS AND METHODS

1. Zebrafish care

Adult wild-type AB zebrafish (*Danio rerio*, 6 months old) were purchased from *European Zebrafish Resource Center* (EZRC, Karlsruhe Institute of Technology (KIT), Kaiserstraße 12, 76131 Karlsruhe, Germany), segregated by sex and housed, at a maximum density of 5 fishes/L, in the fish facility of the *Advanced Technologies Network Center* (ATeN Center, Aut. N. 06/2017-UT 30/03/217) of the Palermo University. Fishes were housed in tanks held in the automatic circulating systems "Tecniplast – ZebTec ActiveBlue Stand Alone" (**Fig. 9a**), with a regulated 14-hour light/10-hour dark cycle, that automatically controls the following parameters: Temperature 28°C, Conductivity 500 ± 50 µS and pH 7,5. The system was periodically provided with 0,6 % Sodium Bicarbonate (Sigma Aldrich) solution and 0,6 % Instant Ocean salt (Aquarium systems) solution, to keep optimal the pH and Conductivity parameters, respectively. They were fed three times a day on a varied diet, with commercial dry fish food (TetraMin flakes, Tetra) supplemented with freshly hatched brine shrimp (Artemia nauplii, Artemia-Hobby), according to standard procedures (*Westerfield, 2007*).

1.1 Zebrafish breeding, embryo harvesting and maintenance

All the experiments described in this thesis were performed exclusively on embryos and larvae within 5 *days post fertilization* (dpf), thus not subjected to animal experimentation rules according to European (2010/63/UE) and Italian (D. lgs. 26/2014) directives.

Adult wild-type AB zebrafish (1 female and 1 male, or 2 females and 2 males) were mated in breeding tanks (**Fig. 9b**) in the late afternoon (06.30 p.m.), separated by a barrier which will be removed the following morning (09.00 a.m.) at the beginning of the light period (*Abdelkader et al. 2013*). Seeded embryos will be released in the bottom part of the tanks, protected by a horizontal dividing grid, which separates them from adult fishes, to prevent them from being devoured. After fertilization, viable normal dividing spherical eggs were washed with 0,1% methylene blue solution, sorted under a stereomicroscope (LEICA MDG41-M80), transferred to a 10 cm Petri

dishes containing 5 ml of E3 embryo medium (5 mM NaCl, 0,17 mM KCl, 0,33 mM $CaCl_2$, 0,33 mM $MgSO_4$, 0,1% methylene blue) and maintained under normoxic conditions at 28°C in the incubator (Fratelli Galli, Control AG-System, G-2100). Embryos were categorized according to *hours post-fertilization* (hpf), dpf, and morphological characteristics (*Kimmel et al. 1995*).


a.
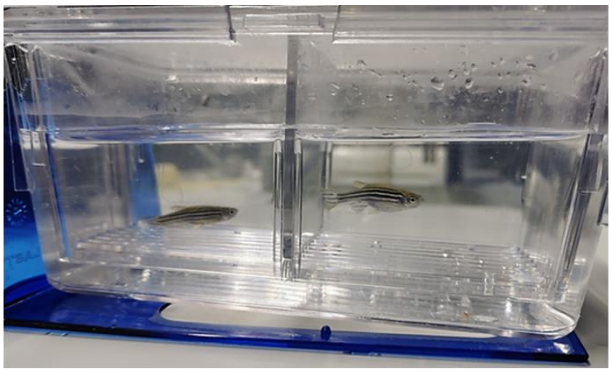
b.

Fig. 9 a, b ***(a)*** *Automatic circulating systems "Tecniplast – ZebTec ActiveBlue Stand Alone".* ***(b)*** *Breeding tanks, with the male on the left and the female on the right.*

1.2 Embryo treatment

Experiments were performed on viable, normal and synchronous embryos. For each type of treatment that will be described, they were sorted 1 embryo/well of a standard 96-well polystyrene microplate (SPL life sciences) in 200 µl E3 medium at the gastrula stage (5.25 hpf) and kept under normoxic conditions at 28°C. The E3 medium was changed daily to avoid contamination and infections spread.

2. Curcumin preparation, treatment, and detection

A 10 mM curcumin stock solution was prepared by dissolving the powder (Merck, Charge/Lot: S4395254-636) in DMSO (Euroclone, EMR031100, Purity: 99.5%). Then, the final concentration treatment solutions (1, 2.5, 5, 7.5 and 10 µM) were properly diluted in embryo medium (E3) and subjected to sonication (TRANSSONIC T310, Elma – Ultrasonic power effective approx.: 35W) for 3 minutes in order to facilitate its solubilisation.

Curcumin treatment started at 6 hpf, the so-called "Shield" stage (when the maternal-to-zygotic transition of gene expression is almost complete) (*Stehr*

et al., 2006; McCollum et al., 2011), and it was administered until 120 hpf (15-20 embryos each, in triplicate). Given the short half-life of curcumin (8 hours in the human organism at 37° C) (*Jäger et al., 2014*), it was chosen to replenish the compound concentration by administration of fresh curcumin-containing medium twice a day (10-14 hours apart, at 08:00 a.m. and 06:00 p.m., respectively).

Treated embryos were compared with the untreated group and with embryos treated with the volume of DMSO, corresponding to the initial volume used to treat embryos with the highest concentration of curcumin (final concentration of 0.1%).

Taking advantage of the curcumin fluorescent property (*Jheng-Yu et al., 2007; Shiau et al., 2011*), it was possible to monitor its absorption and accumulation in the embryos body by microscope observations. Embryos were incubated at 6, 9 and 22 hpf with 0, 1, 2.5, 5, 7.5 and 10 μM curcumin (12 embryos each, in triplicate), and each condition group was observed at 24 hpf using a fluorescence stereomicroscope (Multidimensional Fluorescence Stereomicroscope Leica M205 FA, with Leica DFC 550 camera using Leica LAS X Software), in order to evaluate the fluorescence intensity variations at increasing curcumin concentrations.

In addition, to evaluate the signal saturation, 6 hpf embryos were treated with 5 μM curcumin (12 embryos, in triplicate) and, every 30 minutes, fluorescence images were acquired, up to saturation time. Finally, to evaluate the signal decay, embryos were treated with 5 μM curcumin (12 embryos, in triplicate) at 6, 9 and 22 hpf. At 24 hpf, embryos were washed three times in E3, 5 min each, at *room temperature* (rt). After the last wash the acquisitions started and carried out every 30 minutes, until the complete loss of the fluorescence signal. In both procedures, a parallel set of untreated synchronous embryos were used as a control and for baseline fluorescence evaluation.

3. Radiation setting and treatment

IR treatment (X-rays or protons) was performed at 24 hpf, at rt.

Thanks to the collaboration with the *Medical Physics and Radiation Oncology Department, ARNAS-Civico Hospital (Palermo)*, the Siemens

Primus clinical linear accelerator (Siemens Medical Systems, Concord, CA, USA), which emits photon rays of 6 MV nominal energy, was used to irradiate with X rays. The Linac has been calibrated according to the reference conditions defined by the International Atomic Energy Agency Technical Reports Series No. 398 "Determination of absorbed dose in external beam radiotherapy" (*Technical Reports Series No. 398, IAEA, Vienna, 2000*). Irradiation set up and dose distribution were determined using the Pinnacle treatment planning system (Philips Medical Systems). X-rays treatment was performed using doses of 2, 4, 6, 8, 10, 15 Gy (12-20 embryos each, in quadruplicate), at a dose rate of 200 MU/min. The plates, surrounded by bolus bags (15cm x 15cm x 1.5 cm), were positioned between *polymethyl methacrylate* (PMMA) and CORK slabs, to avoid the sparing effect and to assure an homogeneous radiation exposure (**Fig. 10**). The isocenter was positioned in the plates geometrical centre.

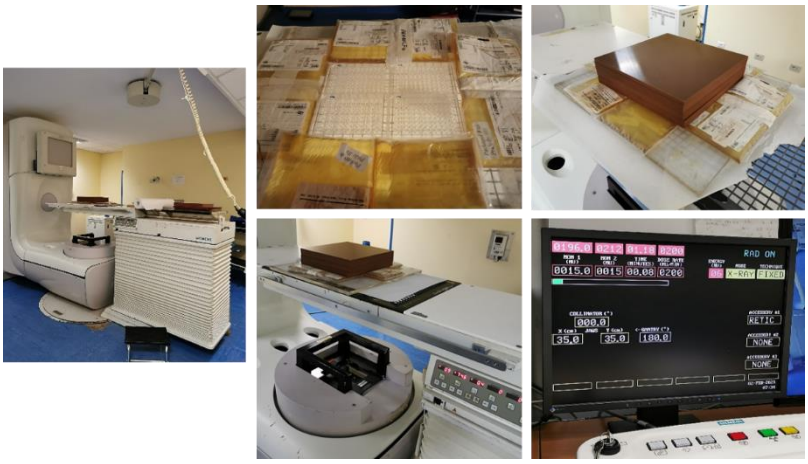

Fig. 10 *On the left the Siemens Primus clinical linear accelerator (Siemens Medical Systems, Concord, CA, USA), from the Medical Physics and Radiation Oncology Department, ARNAS-Civico Hospital (Palermo). On the right the irradiation set up, from the plates positioning - between the slabs - until the setting of the dosimetric parameters.*

One proton irradiation experiment was also performed, using the same range of doses (10 embryos each), after a specific beam time request at the *Protontherapy Center, Trento Hospital (Trento)*, during the PhD visiting period there. The beam has diameter 6x6 cm, with a uniformity ±10%, and a nominal energy of 148 MeV. Irradiation was performed using a dose rate of 2 Gy/min, positioning the target at the middle of SOBP. Due to the beam diameter, each 96-well plates were filled by 1 embryo/well (in 100 µl E3) for

only 30 wells, as a 6 x 5 rectangle in the center of the plate. In addition, considering the horizontal beam orientation, the plate surface has been covered with an adhesive film (Applied Biosystems™ MicroAmp™ Optical Adhesive Film), to avoid the possible E3 dispersion due to the vertical positioning of the plate in a dedicated holder (**Fig. 11**).

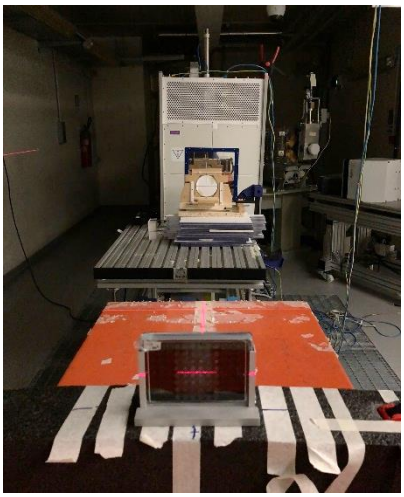

Fig. 11 *Vertical positioning of the 96-well, in a dedicated holder, due to the horizontal beam at the Protontherapy Center, Trento Hospital (Trento).*

4. Combined treatment

6 hpf embryos were treated with 2.5 and 5 μM curcumin (12-20 embryos each, in triplicate). After 18 hours pre-treatment, the same embryos (24 hpf) were subjected to X-rays using the doses of 2, 4, 8, 10 and 15 Gy. After IR treatment, the E3 medium was changed, and the day after all the analysis started. The same protocol was followed for the first, preliminary, combined proton-curcumin treatment (10 embryos each).

5. Experimental workflow for post-treatment toxicological analysis

We devised, in line with what is described in the literature, a multiparametric embryo-larval experimental workflow to evaluate the post-treatment developmental toxicity. The procedure involves the steps described in the figure below, closely related to key time points during embryogenesis (**Fig. 12**).

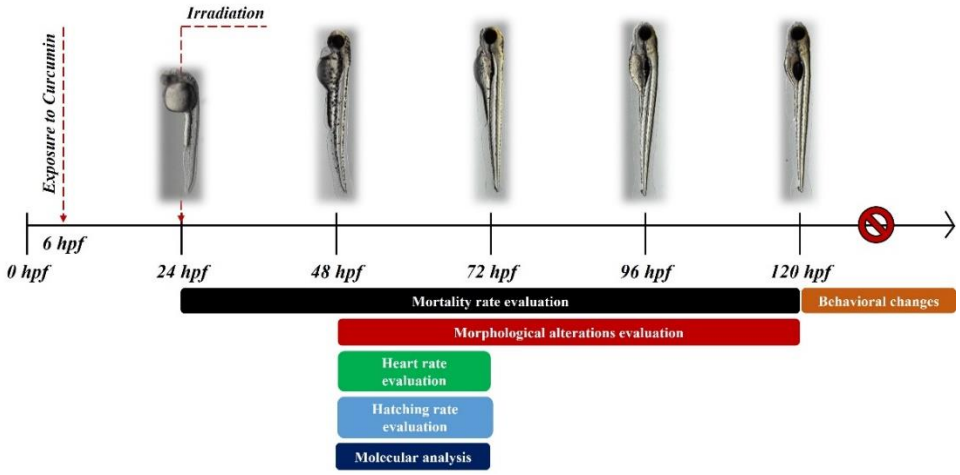

Fig. 12 *Diagrammatic representation of the experimental assays employed in the studies described in this PhD project.*

5.1 Survival and morphology assessments

The assessment of mortality, confirmed by the absence of blood circulation or spontaneous movements within the chorion, started at 24 hpf and was evaluated every 24 hours up to 120 hpf. Survival was calculated as a percentage of viable embryos to the total number of embryos exposed to each treatment group over time (*Wan-Mohtar et al., 2022*).

The search for typical toxicity induced morphological alterations, such as microphthalmia, *Spinal Curvature* (SC), *Pericardial Edema* (PE) and the inhibition of yolk sac resorption (*Yolk Malabsorption*, YM), started at 48 hpf, when there is completion of rapid morphogenesis of primary organ systems, cartilage development in head and pectoral fin, and continued every 24 hours up to 120 hpf (*Kimmel et al., 1995*). Morphology was visually assessed by microscopy and photo-documented every day (Stereomicroscope Leica M205 FA, with Leica DFC 550 camera, using Leica LAS X Software), after anaesthesia with 0.05% (50 mg/L) Tricaine (*3-aminobenzoic acid ethyl ester*) (MS-222 Sigma-Aldrich, CAS no: 886-86-2). Embryo length (from the head tip to the spine end), head and eye length, PE and yolk diameter were properly measured using the image processing program *ImageJ* (*imagej.nih.gov/ij/index.html*) (**Fig. 13**) and were quantified respect to the number of living embryos, in accordance with *Brunner et al., 2020*. The PE diameter values were used to calculate the *Protection Rate* (PR) parameter at 10 Gy, by using the *formula*: [1-(PE measurement in combined treatment/PE measurement in IR treatment) x 100]. Moreover, the PE diameter values were

used for the RBE calculation at 10 Gy, similarly to *Brunner et al., 2020*. In particular, the RBE formula applied was: PE diameter after *IR dose* photons / PE diameter after the same *IR dose* protons.

Fig. 13 *Specific distances considered for the measurement of morphometric parameters: body length in black, yolk sac diameter in blue, eye length in yellow and PE diameter in red. Head lenght measurement not shown.*

5.2 Heart rate evaluation

Despite heart contraction beginning approximately at 24 hpf, heart rate evaluation was evaluated at 72 hpf, when the heart is fully formed and a regular heartbeat is observed (*Vogel and Weinstein, 2000*). Firstly, embryos were put outside the incubator for 20 minutes, to get them used to the rt. Then, they were treated for 20 minutes with 0.05% Tricaine in E3 medium, to prevent movement during the subsequent live acquisitions. Finally, they were placed laterally on a glass slide, each one within a drop of E3, and subjected to 1 minute video capture (Leica DMi8, with Leica DFC365 FX camera, using Leica LAS X Software) for the subsequent manual count of the heart beats (**Fig. 14**). For each experimental condition, 3 videos from different embryos were acquired and manual count was carried out twice by 2 different operators. Mean and *Standard Deviation* (SD) of the values obtained were calculated for each experimental condition under analysis (*Xia et al., 2018*).

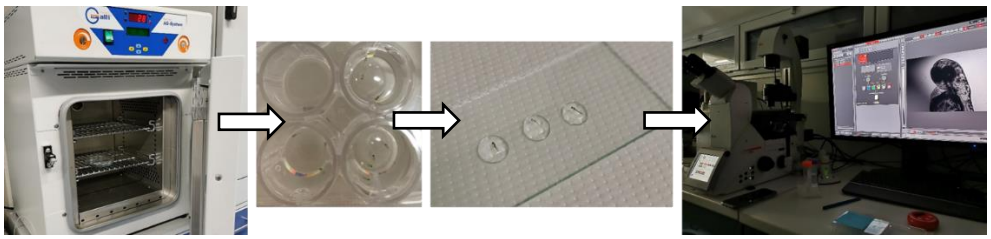

Fig. 14 *Diagrammatic representation of the experimental workflow for the heart rate evaluation, from embryos acclimatization to the heart beats video capture.*

5.3 Hatching rate

Although embryo hatching occurs asynchronously from 48 to 72 hpf, early hatching fish larvae are not more developmentally advanced than those remaining in their chorion. Consequently, the hatching time is not always useful as an index of delayed staging due to a treatment (*Kimmel et al. 1995*).

However, the *Hatching Rate* (HR) was evaluated, at 48 and 72 hpf, in order to deepen the role of this parameter in response to curcumin or IR or both. Hatched embryos percentage was calculated respect to the total number of normal or incubated embryos x 100 (*Samaee et al., 2015*).

5.4 Behavioural analysis

Although during the hatching period the embryo is usually at rest, the early larvae gradually begin to actively swim and produce swift escape responses to seek of prey and feeding (*Kimmel et al., 1995*). For this reason, the evaluation of behavioural changes starts just before 120 hpf.

Alive 118 hpf-larvae were selected and transferred one larva per well in a 96 well-plate in 200 µl of fresh E3 *medium*.

Firstly, at least 3 larvae for experimental conditions were subjected to the *Touch response test analysis* (*Saint-Amant and Drapeau, 1998*), in order to detect qualitatively the individual's reaction to the stimulus, since in its absence the animals remain immobile. Briefly, after the 1-minute interval for acclimatation, a needle stimulus was given and the time of response or the type of movement were observed and video-documented.

Secondly, after an half-hour acclimatization in the incubator, the larvae were positioned inside the ZebraBox observation chamber (*ViewPoint Behavior Technologies, https://www.viewpoint.fr/*) equipped with infrared camera. *Viewpoint* instrument offers the possibility to track the animal activity

through two solutions, a general activity based on pixel changes and a gravity center tracking of each animal, frame to frame, thus leading to a very high accuracy.

After 15 minutes of acclimation into the chamber, the movement of each zebrafish larva (10-12 for each condition, in triplicate) was recorded for 30 minutes. The parameters were set up as follows:

- Colour: black
- Detection threshold: 15
- Movement threshold: Inact/Small = 4 mm/sec. Small/Large = 8 mm/sec
- Time bin: 60 sec
- Light: 50%.

The video was analysed with the appropriate movement tracking software ViewPoint® ZebraLab Tracking Mode (*ViewPoint® Behavior Technologies - version 3.22.3.89*). The raw data and the global path images were processed with ViewPoint® FastData Manager (*version 2.4.0.2510*), in order to evaluate three parameters: 1) average speed (*smlspeed*), 2) small distance (*smldist*) and 3) large distance (*lardist*) (**Fig. 15**). Then, these multiple parameters describe the movement of each larva by the evaluation of the average speed maintained for the selected time period (*smlspeed*), as well as the route type, i.e. short routes through small movements (*smldist*), or long routes through large movements (*lardist*).

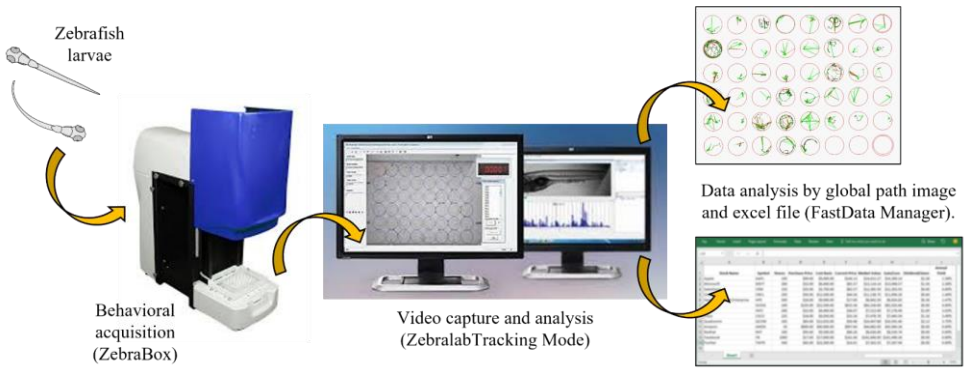

Fig. 15 *Diagrammatic representation of the experimental workflow for the behavioural analysis with ViewPoint® Behavior Technologies (https://www.viewpoint.fr).*

6. Molecular analysis

6.1 Total RNA extraction and reverse-transcription reaction

Total RNA was isolated, for each experimental condition of interest (5 µM curcumin, 10 Gy and 10 Gy + 5 µM curcumin), from 15-25 embryos at 48 hpf, according to the protocol *Purification of Total RNA from Animal Cells using Spin Technology of the RNeasy Mini Kit* (Qiagen). Before starting, embryos were manually dechorionated and deyolked with Deyolking Buffer (55 mM NaCl, 1,8 mM KCl, 1,25 mM NaHCO3).

Each sample was quantified and evaluated (A260/280 and A260/230) by using a spectrophotometer (Thermo Scientific NanoDrop One), with a yield of 10-15 µg of total RNA for each sample. RNA quality was also checked by 1.5% agarose gel electrophoresis.

For the cDNA synthesis, reverse-transcription reactions were carried out following the indications of the *High-capacity cDNA Reverse Transcription kit* (Applied Biosystems). For each sample, the cDNA was synthesized starting from 1 µg of total RNA in reactions of 20 µl. The thermal profile was set up as recommended by the kit:

- 25°C 10’
- 37°C 120’
- 85°C 5’
- 4°C ∞.

6.2 Primer design

Genes of interest were selected for their involvement in oxidative or inflammatory pathways (**Table n. 1**), whereas the Ribosomal protein L13 (*rpl13*) was used as reference gene.

	Name	Abbreviation
Biological process		
Response to oxidative stress	Catalase	*cat*
	Superoxide Dismutase 1	*sod1*
	Superoxide Dismutase 2	*sod2*
	Glutathione Peroxidase 1a	*gpx1a*
	Glutathione Peroxidase 4a	*gpx4a*
	Xanthine Dehydrogenase	*xdh*
	Glutathione S-Transferase Pi	*gstp*
	Glutathione S-Transferase Pi 1a	*gstp1a*
	Lactate Dehydrogenase A	*ldha*
	Signal Transducer and Activator of Transcription 3	*stat3*
Inflammatory response	Interleukin-1β	*il-1β*
	Interleukin-6	*il-6*
	Interleukin-10	*il-10*
	Tumor Necrosis Factor-α	*tnf-α*
Reference gene	Ribosomal protein L13	*rpl13*

Table n. 1 *List of tested targets of interest, classified by pathway to which they belong.*

Information about their gene expression profile was retrieved from *ZFIN* (*https://zfin.org/action/expression/search*). Then, *NCBI* (*http://www.ncbi.nlm.nih.gov/Genbank*) and *Ensembl* (*http://www.ensembl.org/Danio_rerio*) searches in public sequence databases were performed to identify exons sequences for each selected gene. Primers were designed using the *Oligo Explorer Software* (version 1.1.2) and further validated on the *Oligo Analyzer software* (version 1.0.3) to have the following parameters:

- Primer length: 18-22 mer
- Melting temperature: 62°C
- PCR product length: about 150 bp
- ΔG for possible secondary structures: close to 0 kcal/mol.

Each primer sequence was finally checked on the zebrafish genomic reference sequences using *Primer Blast* (*https://www.ncbi.nlm.nih.gov/tools/primer-*

blast/) to exclude non-specific amplification. The respective primer pairs sequences for each gene considered are listed in **Appendix A**.

6.3 Real time quantitative PCR (qPCR)

The cDNA samples were subjected to relative qPCR to compare the expression levels of genes of interest under the various experimental conditions, respect to untreated embryos used as reference. The total reaction volume was 20 µl, with the following specifications: 10 ng cDNA, 0.2 µM Primer FW/RW, 10 µl 5X Fast SYBR® Green (Applied Biosystems). The thermal profile was set up as default:

- *Stage 1, Reps:1* 95°C 20''
- *Stage 2, Reps:40* 95°C 03'' - 60°C 30''
- *Stage 3, Reps:1* 95°C 15'' - 60°C 1' - 95°C 15''.

Each reaction was performed in triplicate in *StepOnePlus™ Real-Time PCR System, 96 well Thermal* Cycler (Applied Biosystem). ROX dye was used as passive reference and a *Non-Template Control* (NTC) was added for each primers pair.

At the end of the Real-Time PCR reaction (*Stage 3*), a dissociation curve analysis was performed to confirm the PCR amplicons homogeneity.

7. Statistical analysis

Statistical data assessment was performed using *GraphPad Instat (Version 3.05)*.

Differences between observed and expected distributions between two groups of values were evaluated by using a contingency table (two rows, two columns) and a Fisher's exact test, to calculate the *p value* (*p*) and the *Odds ratio* (OR) with 95% *Confidence interval* (CI). This approach was used for the significance evaluation of malformation rates (%) at 120 hpf, in pre-treated embryos *vs* the only irradiated ones for each dose (2-10 Gy), and to compare the SC or PE incidence at 96 hpf in pre-treated embryos *vs* the only irradiated ones for each dose (10-15 Gy).

On the other hand, *one-way analysis of variance (ANOVA)* was used to analyse if variation among variables means is significantly greater than expected by chance. In particular, it was applied to evaluate means of the morphometric parameter PE, obtained for pre-treated embryos *vs* the only irradiated ones, at 72 and 96 hpf for each dose used (10-15 Gy).

Overall, statistical significance was defined at $p \leq 0{,}05$.

RESULTS

1. Curcumin treatment

Curcumin (cur) auto-fluorescence was evaluated at 24 hpf for all treatment conditions. This allowed to confirm the molecule absorption by embryos and to evaluate quantitative differences between the various concentrations used, through the measurement of emitted fluorescence intensity. As shown in **Fig. 16**, fluorescence signal started to be observed from 2.5 µM curcumin, becoming evident at 5 µM concentration. Signal intensity occurred in a dose-dependent manner, and no background fluorescence was detected in curcumin solutions, suggesting that most of the compound decomposed in the E3 aqueous solution (*Wu et al., 2007*).

Considering the prevalent area of the fluorescence signal, curcumin would appear to accumulate in the yolk sac.

The fluorescence saturation and decay time showed, respectively, a time window of 5 and 6 hours.

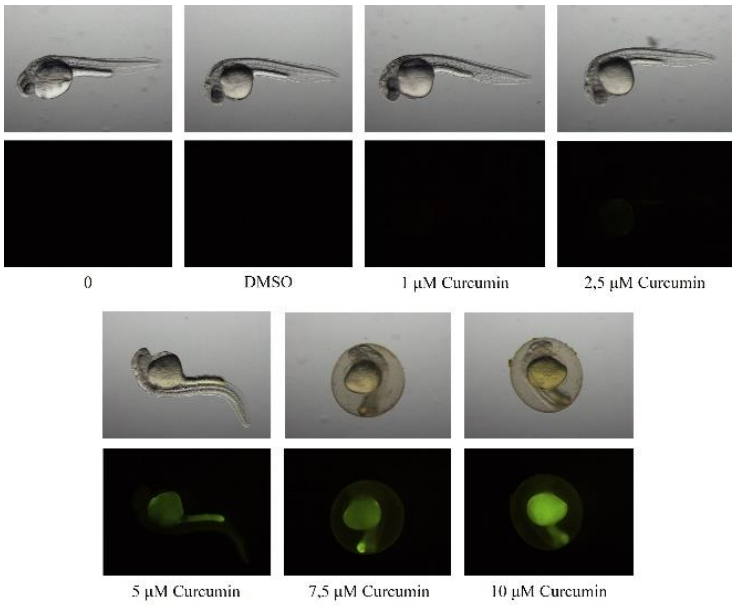

Fig. 16 *Accumulation of curcumin (1-10 µM) in 24 hpf zebrafish embryos. Pictures were taken in light field and in fluorescence field.*

Embryos were observed every 24 hours until the 120 hpf stage, evaluating the survival rate and phenotypic changes; data presented as the mean of 3 experiments are summarised in **Fig.17-20**.

Curcumin exposure, twice a day for 5 days, inflicted gross malformations in a dose-dependent manner from 5 µM onwards, being 100% lethal at concentrations of 7.5 and 10 µM at 72 and 48 hpf, respectively. For the remaining concentrations, a lower mortality of 31%, 26% and 46% was detected at 120 hpf for embryos exposed to 1, 2.5 and 5 µM, respectively, *versus* (*vs*) a 30% baseline mortality observed in the control embryos (**Fig. 17**).

The number of embryos showing one or more morphological abnormalities appears to be prevalent from 5 µM onwards, with values ranging from 12% to 47% at 24 and 120 hpf, respectively, against less than 1% baseline alterations observed in the control embryos (**Fig. 17**).

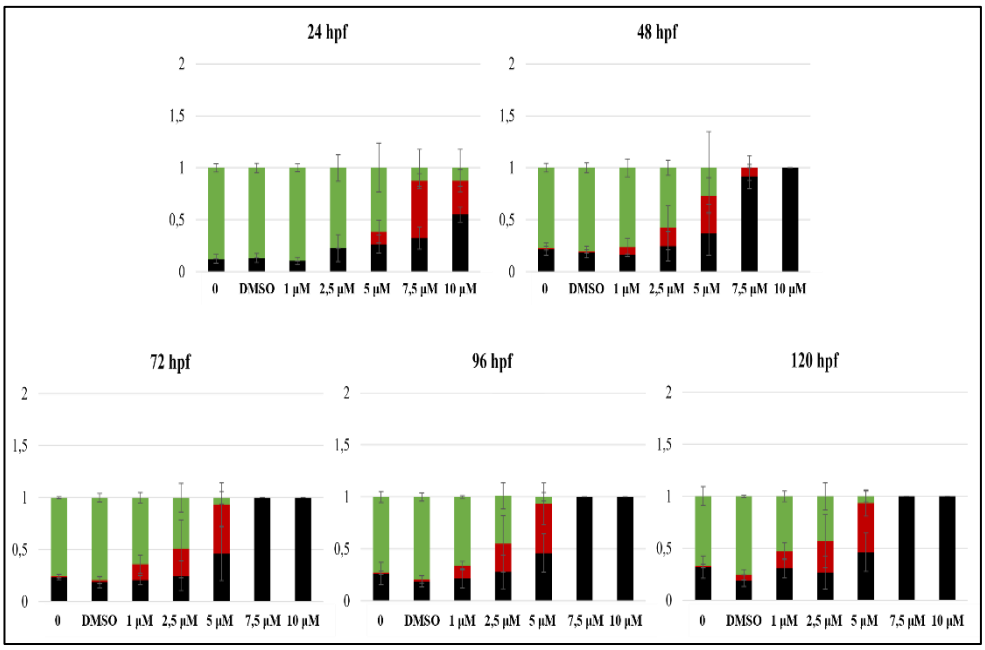

Fig. 17 *Normal (green bar), dead (black bar) and abnormal (red bar) embryos rates in developing zebrafish embryos exposed to 0, 1, 2.5, 5, 7.5 and 10 µM of curcumin. Data are presented as the mean of 3 experiments. Error bar = ± SD.*

Among the main alterations under analysis (within the fraction of the malformed embryos), SC prevailed; it appeared since 24 hpf in embryos treated with 5 µM and the number of affected specimens increased up to 72% at 120 hpf. Fewer embryos appeared to be affected by exposure to lower concentrations of 1 and 2.5 µM curcumin from 48 hpf, with a maximum incidence of 66% at 120 hpf. PE, the alteration most incompatible with embryonic survival was also observed, with an incidence of 40% already

appearing at 48 hpf with 5 µM curcumin. A lower degree of *Pigmentation* (PIGM) as well as cases of developmental delay – related to YM - were also found in samples treated with 5 µM curcumin, starting from 48 hpf and 24 hpf, respectively (**Fig. 18-19**).

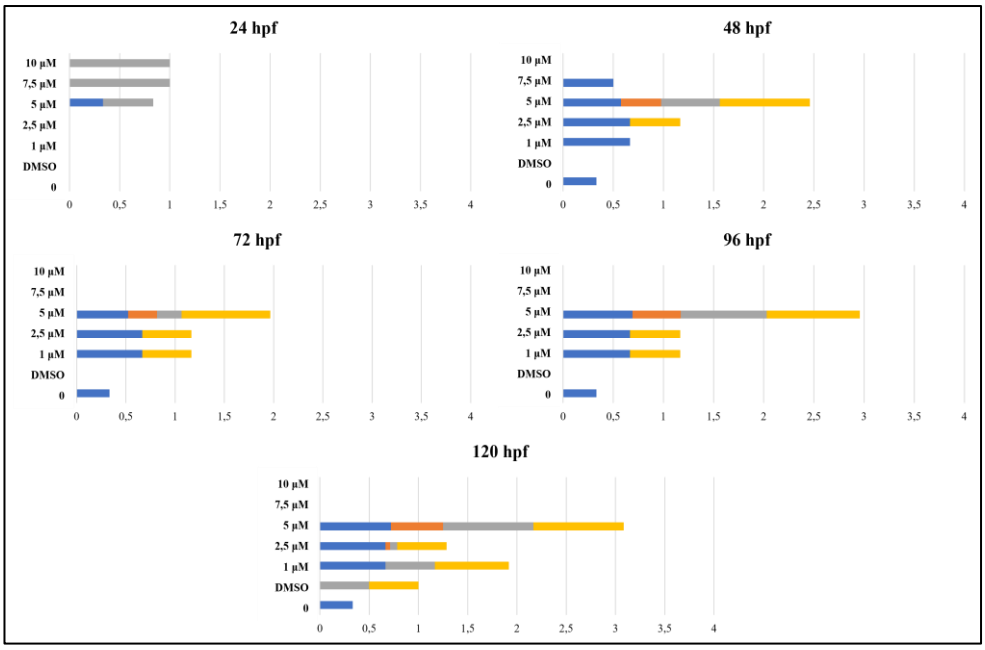

Fig. 18 *Distribution (%) of the main malformations observed in malformed developing zebrafish embryos exposed to the experimental concentrations of curcumin: SC (blue bar), PE (orange bar), YM (gray bar), PIGM (yellow bar). Data are presented as the mean of 3 experiments.*

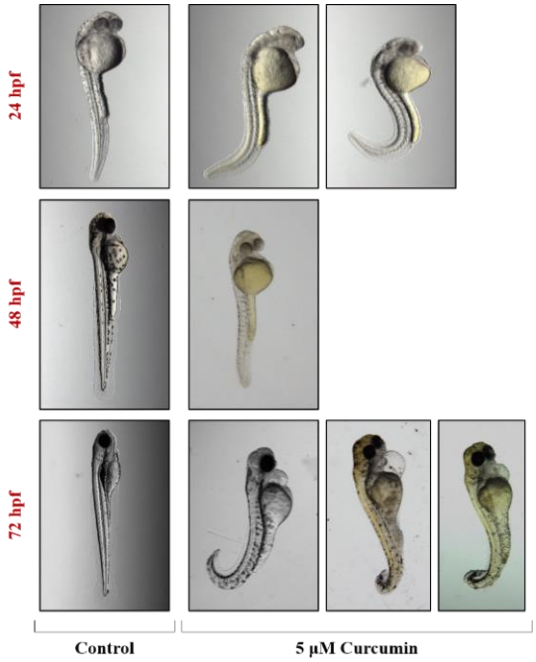

Fig. 19 *Representative images of the main malformations observed after treatment with 5 µM curcumin, such as YM (from 24 hpf), SC (from 24 hpf), PE (from 72 hpf), PIGM (from 48 hpf). Pictures were taken in light field.*

The hatching rate analysis showed that the treatment with 5 µM curcumin, compared to untreated controls, led to a delay of the phenomenon at 48 hpf (37,5% *vs* 93%), which was then recovered at 72 hpf.

The behavioural analysis was performed at 120 hpf, through the use of the *touch-evoked escape response assay*. For concentrations ≤ 2.5 µM the response was similar to controls, while it was clearly reduced for embryos treated with 5 µM curcumin, probably due to the severity of morphological abnormalities, such as SC. This analysis, further improved using the ZebraBox platform *(ViewPoint Behaviour Technology)*, showed that curcumin did not induce significant alterations in the locomotor activity of treated embryos compared to controls, in particular regarding the mean velocity (*smlspeed*) parameter, according to literature (*Bertoncello et al., 2018*) (**Fig. 20**).

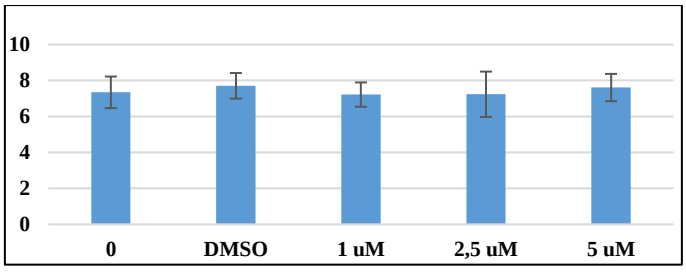

Fig. 20 *Curcumin treated 120-hpf larvae smlspeed during a 30 minutes assay. Data are reported as the mean of 10-12 120 hpf-larvae per experiment. Raw data were processed with ViewPoint® FastData Manager (version 2.4.0.2510) and the charts drawn with Microsoft Excel 2016. Y axis: mm/sec. Error bar = ± SD.*

The observation of blood circulation, as well as the manual evaluation of the heart-beating rate, did not reveal any dysfunction in treated embryos compared to controls. Only a slight increase (1%) in heart-beating rate was observed, at 72 hpf, with 2.5 and 5 µM curcumin.

2. Irradiation treatment with conventional X-rays

Daily assessment of irradiated embryo viability, morphological alterations and behavioural defects showed a correlation with the radiation dose. Data

presented are the mean of 4 experiments, and they are summarised in **Fig.21-23**.

IR treatment led to a very low mortality for embryos exposed from 2 to 15 Gy X-rays than the untreated ones, but inflicted malformations in a dose-dependent manner. Gross alterations were observed from 8 Gy onwards with incidences of 50% and 82% in 15 Gy treated embryos at 48 and 120 hpf, respectively, *vs* a 3% baseline of malformations incidence in the controls (**Fig. 21**).

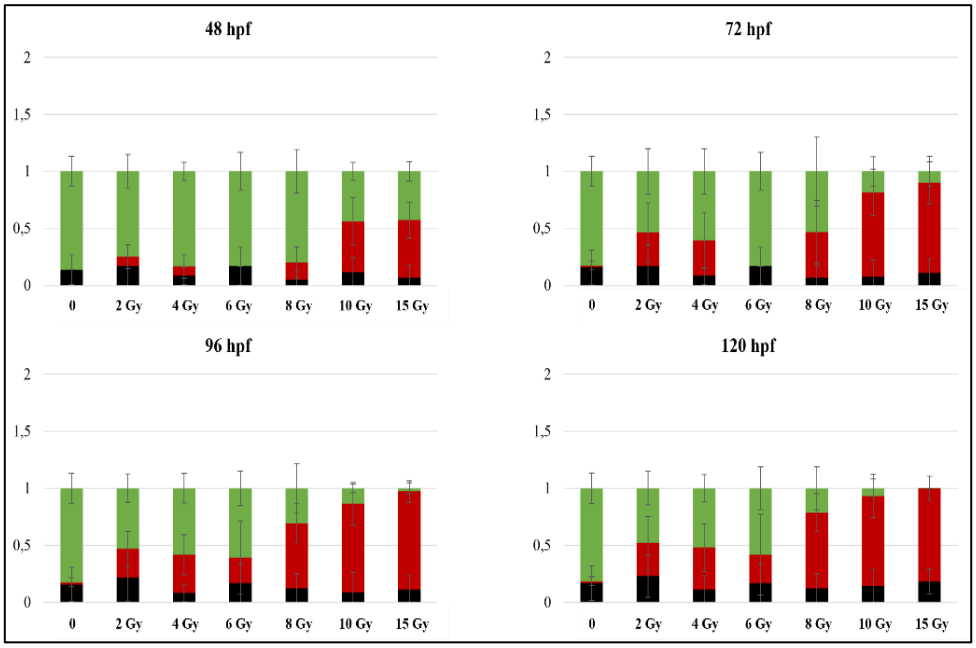

Fig. 21 *Normal (green bar), dead (black bar) and abnormal (red bar) embryos rates of developing zebrafish embryos exposed to the doses of 0, 2, 4, 6, 8, 10, 15 Gy of X-rays. Data are presented as the mean of 4 experiments. Error bar = ± SD.*

Within the fraction of malformed embryos, PE prevailed for the higher doses. It appeared since 48 hpf in embryos treated with the doses of 10 and 15 Gy (with an incidence of 10 and 25%, respectively), or since 72 hpf in embryos treated with lower doses, with a final percentage of affected specimens of 62% and 98% in embryos treated with the doses of 10 and 15 Gy, respectively, at 120 hpf. By contrast, fewer embryos appeared to be affected by exposure to lower doses than 8 Gy, with a maximum of 18% with 2 Gy at 120 hpf. SC was also observed, starting at 48 hpf in embryos treated with 8, 10 and 15 Gy (16%, 38% and 49%, respectively) or at 72 hpf using lower

doses. YM and PIGM were also found starting from the 2 Gy dose, already at 48 hpf (**Fig. 22**).

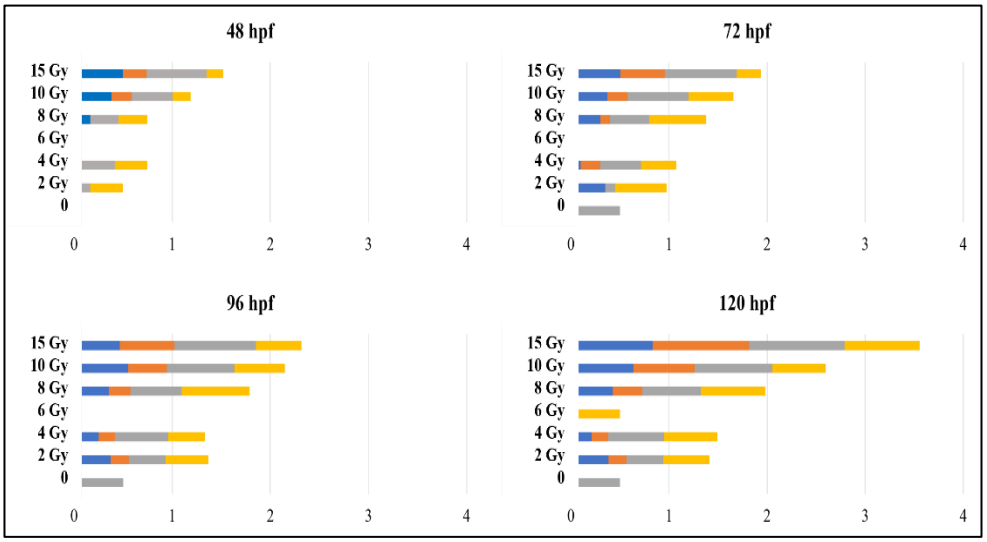

Fig. 22 *Distribution (%) of the main malformations observed in malformed developing zebrafish embryos exposed to the experimental doses of 0, 2, 4, 6, 8 and 15 Gy of X-rays: SC (blue bar), PE (orange bar), YM (gray bar), PIGM (yellow bar). Data are presented as the mean of 4 experiments.*

The hatching rate analysis showed that the IR treatment delayed this phenomenon, in comparison to untreated controls, in a dose-dependent manner. Indeed, at 48 hpf the rate of hatched embryos was 86% and 39% for 2 and 15 Gy, respectively, *vs* 100% in controls. This delay was recovered at 72 hpf for doses lower than 6 Gy, but not for specimens treated with 8-15 Gy of IR, which conserved a certain rate of developmental delay even after 72 hpf.

The behavioural analysis of 120 hpf larvae, performed using the *touch-evoked escape response assay*, showed that the response was similar to controls for doses ≤ 8 Gy, while it was clearly reduced for embryos treated with 10 and 15 Gy. This analysis, further improved using the ZebraBox platform *(ViewPoint Behaviour Technology)*, showed that IR treatment did not induce significant alterations in the locomotor activity of IR treated embryos, compared to controls, specifically on the mean velocity (*smlspeed*) parameter (**Fig. 23**). Instead, a difference was observed in the type of travelled distance (*dist*) parameter, specifically in the small (*smldist)* and large (*lardist)* distance, associated to short or long routes, respectively. Indeed, the irradiated

embryos prefer to cross small distance than large ones, respect to the controls. For the dose range of 2-10 Gy it was observed an increase in the *smldist* values ranging from + 30,25 to + 150,86 mm, and a reduction in the *lardist* values, ranging from - 0,1 to - 7,12 mm.

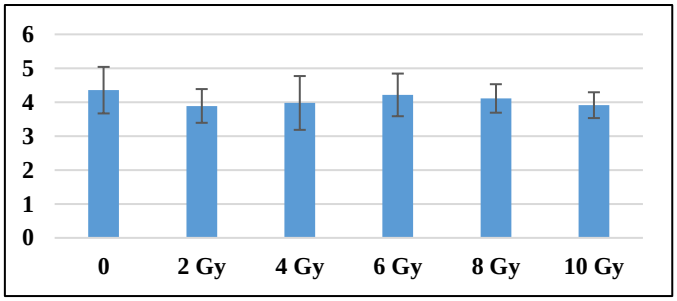

Fig. 23 *IR treated 120 hpf -larvae smlspeed during a 30 minutes assay. Data are reported as the mean of 10-12 120 hpf-larvae per experiment. Raw data were processed with ViewPoint® FastData Manager (version 2.4.0.2510) and the charts drawn with Microsoft Excel 2016. Error bar = ± SD.*

The observation of blood circulation, as well as the manual evaluation of the heart-beating rate, revealed a small decrease (in the range from - 6% to - 22%), in a dose-dependent manner, in treated embryos compared to controls. Unexpectedly, a slight increase was observed at 15 Gy (+ 9,8%).

3. Curcumin-X rays combined treatment

Based on the results obtained with the curcumin treatment, the non-toxic concentrations of 2.5 and 5 µM were chosen to test the role of curcumin pre-treatment in combination with the 0-15 Gy range of an IR conventional X-rays treatment. Data presented are the mean of 3 experiments, and they are summarised in **Fig. 24-32**.

Irradiated embryos viability was not significantly affected by the 18 hours pre-treatment with 2.5 and 5 µM curcumin, respect to the controls; this was expected, considering the low mortality given by radiation treatment alone in the selected dose range.

Instead, pronounced protective effects were found in the percentage of malformed embryos, after combined treatments using both the chosen curcumin concentrations, respect to the only irradiated embryos. Notably, this effect is visible in the 2-10 Gy range, and it is greater for the higher

concentration of curcumin (5 µM). Specifically, at 120 hpf, the 5 µM curcumin pre-treatment led to a reduction of malformations percentages respect to those of IR treatment alone, as following reported for each dose:

- 2 Gy: 22% *vs* 41% (*p*: 0,0017; OR: 0,3577; 95% CI: 0,1880 to 0,6808);
- 4 Gy: 35% *vs* 49% (*p*: 0,2255; OR: 0,6687; 95% CI: 0,3678 to 1,216);
- 8 Gy: 52% *vs* 63% (*p*: 0,0057; OR: 0,4127; 95% CI: 0,2198 to 0,7749);
- 10 Gy: 66% *vs* 87% (*p*: 0,0002; OR: 0,2093; 95% CI: 0,08982 to 0,4876).

Instead, at the highest dose of 15 Gy a slight protective effect is exerted up to 96 hpf (87% *vs* 91%) (*p*: 0,0658; OR: 0,3187; 95% CI: 0,09897 to 1,026), which disappear at 120 hpf (**Fig. 24, Appendix B**).

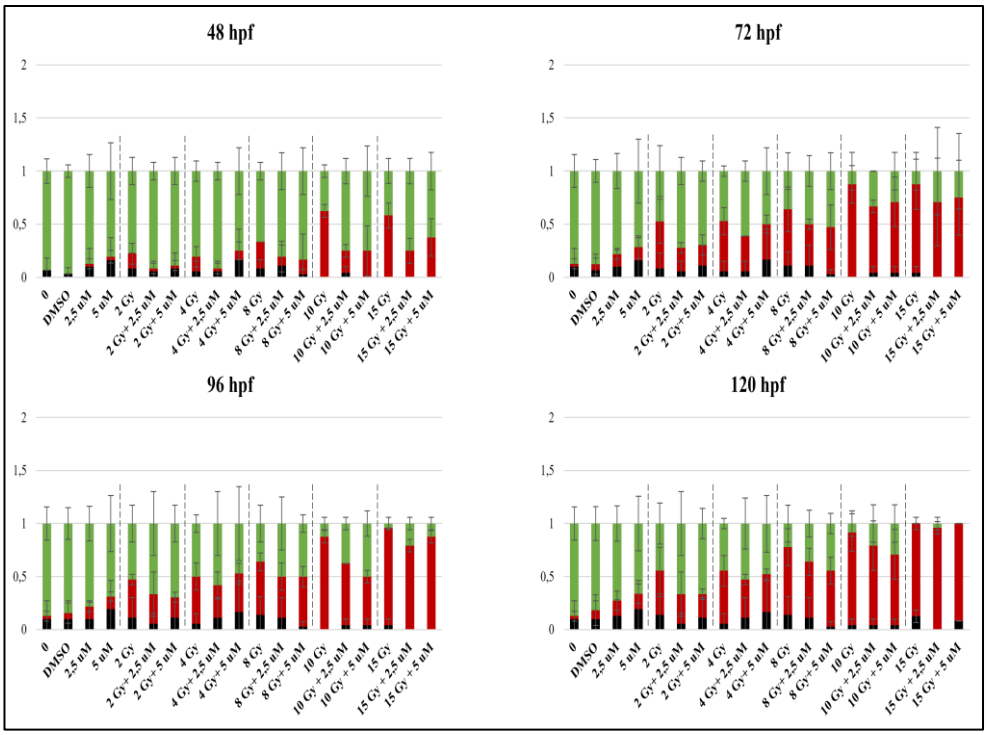

Fig. 24 *Normal (green bar), dead (black bar) and abnormal (red bar) embryos rates of developing zebrafish embryos exposed to a combination of curcumin pre-treatment with concentrations of 2.5 or 5 µM, followed by irradiation with 0, 2, 4, 8, 10 or 15 Gy of X-rays. Data are presented as the mean of 3 experiments. Error bar = ± SD.*

The most important morphological abnormalities, PE and SC, prevailed for the higher doses (10 and 15 Gy), and in both experimental conditions their incidence decreases up to 96 hpf, in the presence of curcumin pre-treatment and in a dose-dependent manner. In detail, the incidence of SC at 96 hpf was 55% and 56% in samples treated with 10 and 15 Gy, respectively, *vs* 40% and 42% for the 5 µM pre-treated embryos for the same IR doses (10 Gy: *p*:

0,0472; OR: 0,5455; 95% CI: 0,3111 to 0,9565. 15 Gy: *p*: 0,0657; OR: 0,5690; 95% CI: 0,3250 to 0,9962). The same trend is observable at the same time point for the PE, as its incidence was 48% and 70% in samples treated with 10 and 15 Gy respectively, *vs* 25% and 48% in the presence of 5 µM curcumin pre-treatment (10 Gy: *p*: 0,0012; OR: 0,3611; 95% CI: 0,1984 to 0,6574. 15 Gy: *p*: 0,0024; OR: 0,3956; 95% CI: 0,2214 to 0,7069). Furthermore, despite the low incidence of these serious malformations at lower doses, the protective effect of curcumin was also confirmed with lower doses of IR. Indeed, the PE incidence at 96 hpf in 4 Gy treated embryos was of 11% *vs* 0% in the combined treated group with 2.5 and 5 µM curcumin, whereas it was 14.6% in 8 Gy treated specimens *vs* 0.06% and 0% in the combined treated group with 2.5 and 5 µM curcumin (**Fig. 25-26 a, Appendix B.1**).

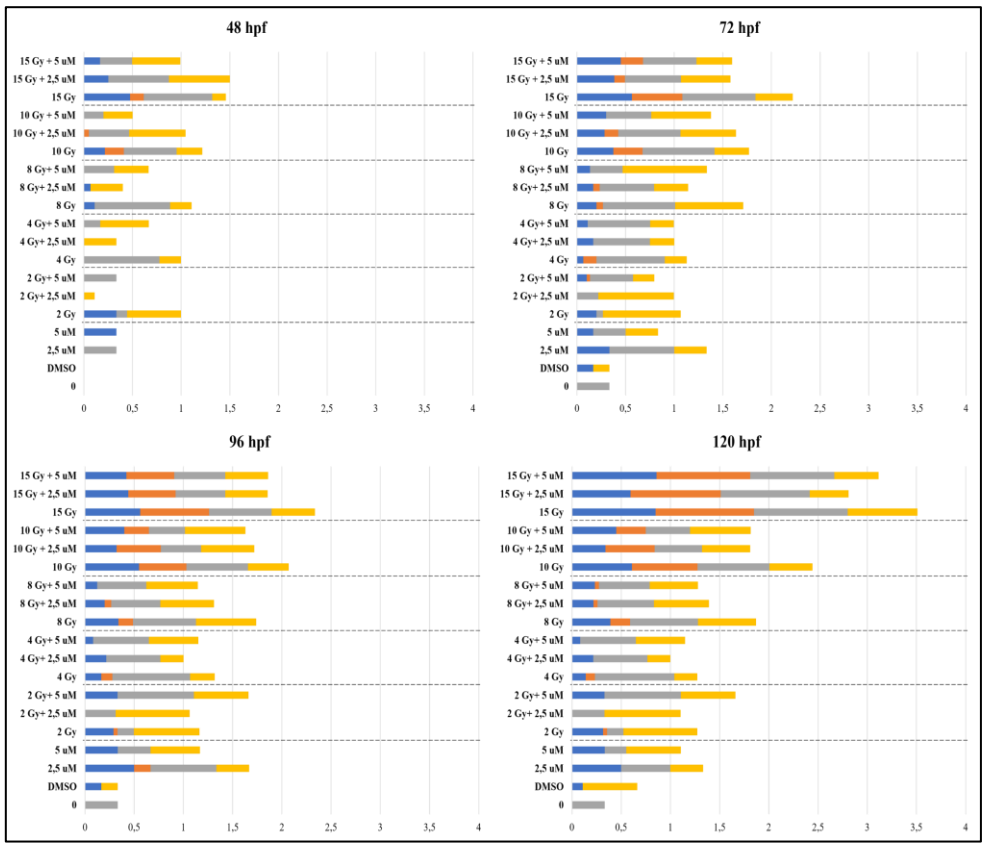

Fig. 25 *Distribution (%) of the main malformations observed in malformed developing zebrafish embryos exposed to a combination of curcumin pre-treatment with concentrations of 2.5 or 5 µM, followed by irradiation with 0, 2, 4, 8, 10 or 15 Gy of X-rays: SC (blue bar), PE (orange bar), YM (gray bar), PIGM (yellow bar). Data are presented as the mean of 3 experiments.*

Noteworthy and mainly noticed for the higher radiation doses, the degree of phenotype severity of a certain malformation observed per each IR dose, was generally reduced in embryos pre-treated with curcumin respect to the IR treamtent alone (**Fig. 26 b**).

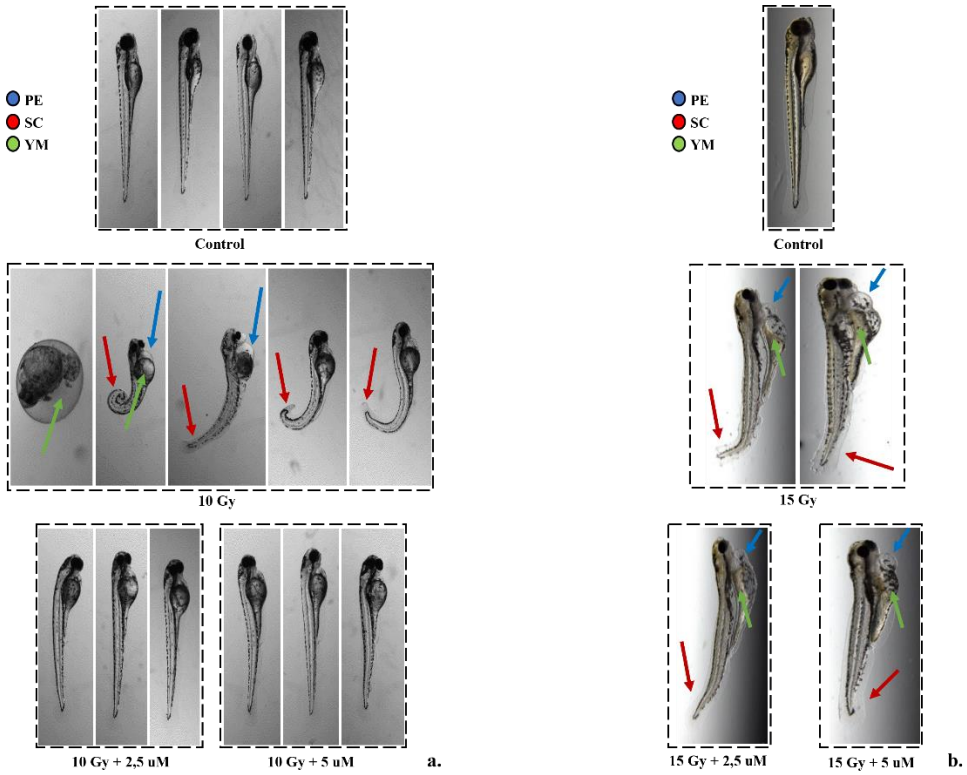

Fig. 26 a, b. *Representative images of the main malformations (PE, SC, YM) observed, at 120 hpf, after treatment with 10 Gy (**a**) or 15 Gy (**b**) alone or combined with both 2.5 and 5 μM curcumin concentration, vs controls.*

In particular, the evaluation of morphometric parameters at 72 and 96 hpf, such as body length, yolk sac diameter, eye length and head length, confirmed - at different extent - the protective effect exerted by the curcumin pre-treatment for higher doses of radiation (10 and 15 Gy) (**Fig. 27 a, b**).

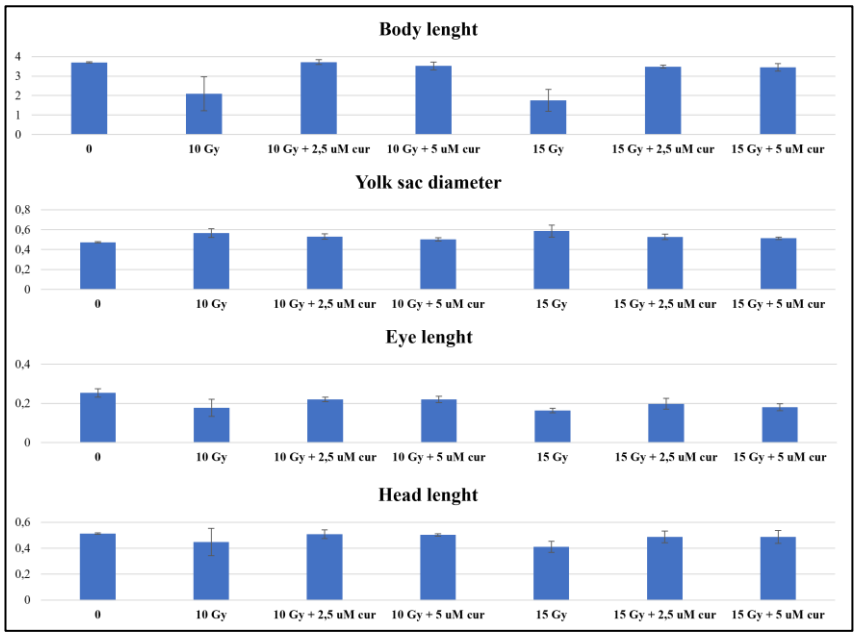

a.

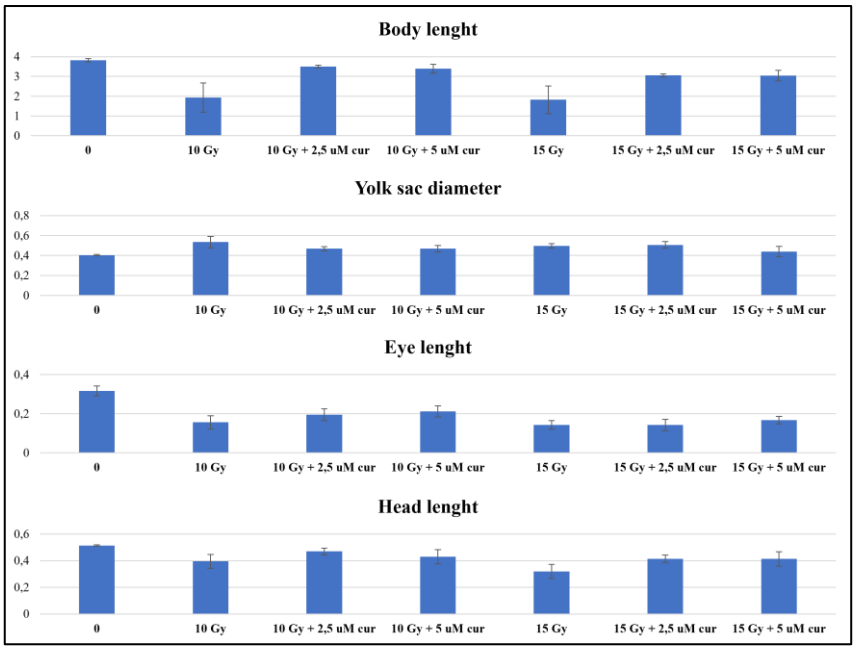

b.

Fig. 27 a, b *72 (**a**) and 96 (**b**) hpf measurement (mm) of morphological parameters (body length, yolk sac diameter, eye length and head length) after 10 and 15 Gy of IR treatment, with or without curcumin 2.5 and 5 µM pre-treatment. Error bar = ± SD.*

Even more interesting, the PE measurement, for the same treatments at the same time points, showed values of 0,14 and 0,15 mm at 72 hpf with 10 and 15 Gy, and 0,16 and 0,20 mm at 96 hpf with the same doses, respectively. Instead, in pre-treated embryos with 2.5 or 5 µM curcumin, the 72-hpf PE values were 0,085 and 0,01 mm with the dose of 10 Gy (*p*: 0,0014) and 0,067 and 0,11 mm with the dose of 15 Gy (*p*: 0,0127), respectively, while the 96-

hpf PE values were 0,08 and 0,12 with the dose of 10 Gy (*p*: 0,0052) and 0,09 and 0,1 with the dose of 15 Gy (*p*: 0,0001) (**Fig. 28**).

In order to quantify the curcumin protection ability, a *Protection Rate* (PR) has been calculated as described in materials and methods and values are reported in **Table n. 2**.

Pre-treatment with the lower curcumin concentration (2.5 µM) led to an higher reduction in the PE diameter, respect to those observed with the 5 µM curcumin pre-treatrement, offering higher rates of protection, comparing the same time point of 72 hpf or 96 hpf, in 10 Gy irradiated embryos.

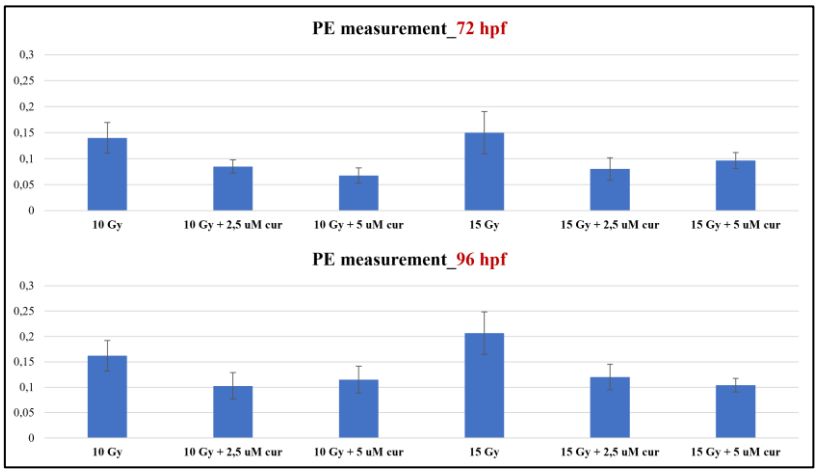

Fig. 28 *72 and 96 hpf measurement (mm) of PE parameter after 10 and 15 Gy of IR treatment, with or without curcumin 2.5 and 5 µM pre-treatment. Error bar = ± SD.*

	72 hpf	96 hpf
10 Gy + 2,5 µM	39,28%	50%
10 Gy + 5 µM	28,57%	25%

Table n. 2 *Protection Rate (PR) values (%), for 10 Gy dose, with both concentration of curcumin, at 72 and 96 hpf, respectively.*

In addition, the manual evaluation of the heart-beating rate at 72 hpf revealed a decrease in the only irradiated embryos compared to controls, from 2 to 10 Gy (**Fig. 29**). Curcumin pre-treatment, at both concentrations and better with the lower one, seems to exercise a protective role, bringing the heartbeat values closer to those of the controls for the same doses. Instead, the embryos treated with dose of 15 Gy with or without curcumin soffer of increased

heartbeat, as the PE volume is more pronounced, so that the heart try to compensate with an increased heart frequency.

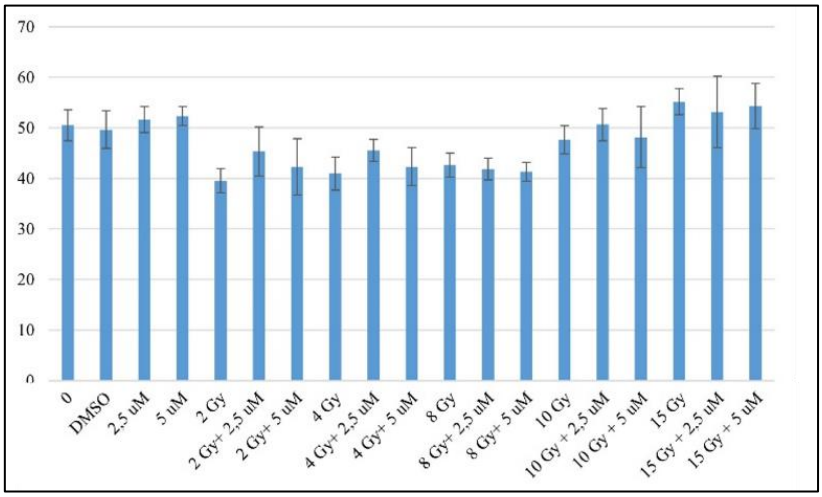

Fig. 29 *Heart rate values (bpm) of 72 hpf embryos exposed to to the experimental doses of 0, 2, 4, 8 and 15 Gy of X-rays in combination with 2.5 or 5 μM curcumin pre-treatment. Data are presented as the mean of 3 experiments. Error bar = ± SD.*

Behavioural analysis using the ZebraBox platform *(ViewPoint Behaviour Technology)* was performed at 120 hpf, on non-morphologically compromised larvae (0-10 Gy). The results showed that in the dose range under analysis there was not a significant alteration of the average speed (*smlspeed*) maintained by the treated embryos, both with IR or combined treatment, than the controls (**Fig. 30**). Furthermore, as above already reported, an increase in the *smldist* parameter and a decrease in the *lardist* parameter was observed in the only irradiated embryos than the control ones. However, the curcumin pre-treatment seems to correct this abnormal larvae behavior. For doses range 2-10 Gy a lower increase in the *smldist* values was observed in pretreated embryos respect to controls (variations from + 0,32 to + 61,19 mm), than *smldist* variations previously described for the only irradiated ones. A parallel increase in the *lardist* values was also observed for doses ≥ 8 Gy respect to controls, with variations ranging from + 6,85 to + 10,7 mm, compared to what was previously observed in only irradiated embryos.

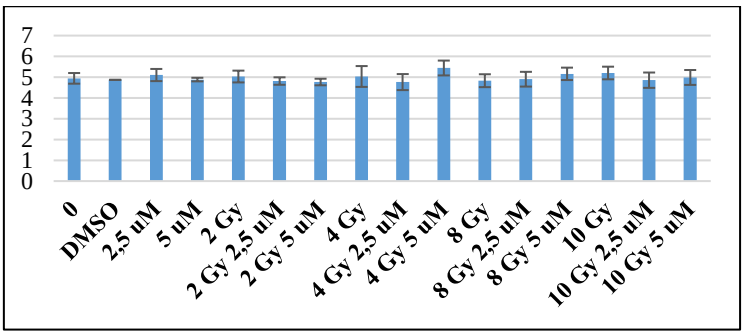

Fig. 30 *IR and combined treated 120 hpf -larvae smlspeed during a 30 minute assay. Data are reported as the mean of 10-12 120 hpf-larvae per experiment. Raw data were processed with ViewPoint® FastData Manager (version 2.4.0.2510) and the charts drawn with Microsoft Excel 2016. Error bar = ± SD.*

Molecular analyses were focused on some targets mainly involved in oxidative stress and inflammation, which are tightly related to IR induced toxicity in normal tissue (**Table n. 1**). We used, for both panels, 48 hpf embryos, i.e. the 24 hours post radiation treatment timepoint, as used in previous *in vitro* studies already mentioned (*Minafra et al, 2019*). Moreover, *a priori* we have chosen to analyse the gene expression in embryos treated with 10 Gy and 5 μM curcumin, as these could be supposed more stressful treatments. **Fig. 31-32** shows the mRNA relative expression of the selected target genes in the above mentioned samples, normalized respect to untreated controls and using *rpl13* as a endogenous gene.

Only IR treatment led to a lowering of expression levels, with different entity, of all the antioxidant enzymes under analysis. Overall, the trend observed is similar for all the genes analysed. Indeed, the treatment with IR produced a decrease in the mRNA level of the antioxidant gene targets, whereas their levels were higher in embryos treated with 5 μM curcumin. Interestingly, in combined treated embryos, the mRNA levels of these antioxidant genes were restored close to those of untreated samples. The following are the gene expression levels induced by combined *vs* IR treatment for each gene under study: *cat* 1,10 *vs* 0,70, *sod1* 1,04 *vs* 0,63, *gpx4a* 0,74 *vs* 0,37, *gpx1a* 1,08 *vs* 0,81, *xdh* 1,13 *vs* 0,77, *sod2* 1,56 *vs* 0,44, *gstp* 1,33 *vs* 0,88, *gstp1a* 1,32 *vs* 0,98, *ldha* 2,07 *vs* 0,33 and *stat3* 1,27 *vs* 0,92 (**Fig. 31**).

Fig. 31 *Genes expression variation of targets involved in oxidative stress regulation, in embryos treated with 5 µM curcumin and 10 Gy, as single or combined treatments, analysed by qPCR. Reference sample (Control) =1. Error bar = ± SD.*

Regarding the inflammatory panel, we have chosen to analyse the gene expression of the main pro-inflammatory cytokines as *il-1β*, *il-6*, *tnf*-α, and *il-10* as the main anti-inflammatory one.

Interestingly, the four targets chosen showed a similar trend. Indeed, their expression levels were lower than that of untreated embryos (lower than 1) in any treatment studied. However, the combined treated embryos showed higher expression level of these four cytokines (*fold change* value of 0,93, 0,90, 0,57 and 0,53 for *il-1β*, *il-6*, *tnf-α* and *il-10*, respectively) compared to that of solely IR and curcumin treated embryos (**Fig. 32**).

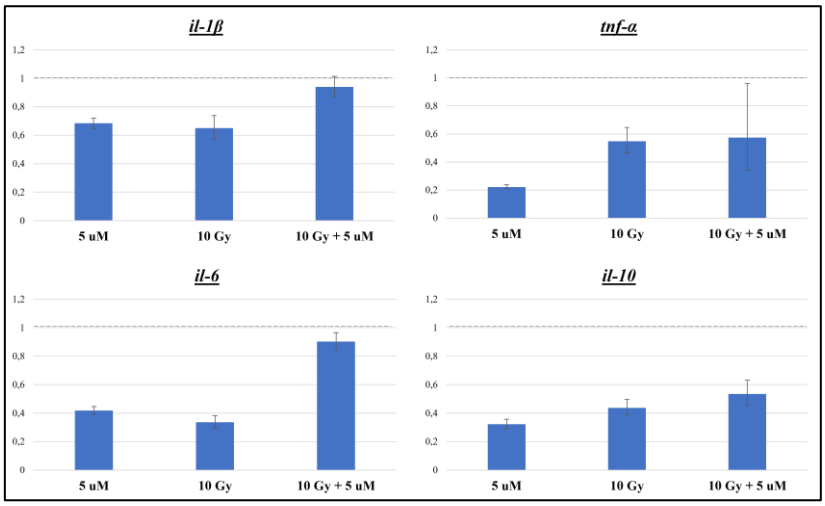

Fig. 32 *Genes expression variation of target genes involved in inflammation, in embryos treated with 5 µM curcumin and 10 Gy, as single or combined treatments, analysed by qPCR. Reference sample (Control) =1. Error bar = ± SD.*

4. Curcumin-Protons combined treatment

Daily assessment of irradiated embryo viability, morphological alterations and cardio-circulatory system defects showed a correlation with the radiation dose. Data presented derived from one preliminary experiment, and they are summarised in **Fig. 33-37.**

Protons treatment led to a very low mortality for embryos exposed from 2 to 15 Gy, compared to the untreated ones, with a maximum death of 9% for the higher doses (10 and 15 Gy) at 120 hpf. The 2.5 and 5 µM curcumin pre-tratment led to 0% dead embryos at the same time point with the same doses. In proton-treated embryos, malformations increased in a dose-dependent manner and constantly from 72 up to 120 hpf. The highest percentages of malformed embryos range from 75% with the 4 Gy dose to 91% with the 10 and 15 Gy doses at 120 hpf. Curcumin pre-treatment, in a concentration-dependent manner, reduced the percentages of malformed embryos at 120 hpf, with percentage values of: 58% and 33% with 2.5 and 5 µM of curcumin and the dose of 4 Gy, respectively, and 66% with both curcumin concentrations with the 10 Gy dose. Instead, in embryos treated with the highest dose of 15 Gy, the toxic effect induced by IR prevailed, as the pre-treatment with 2.5 µM of curcumin led to a slight protection only up to 96 hpf (**Fig. 33**).

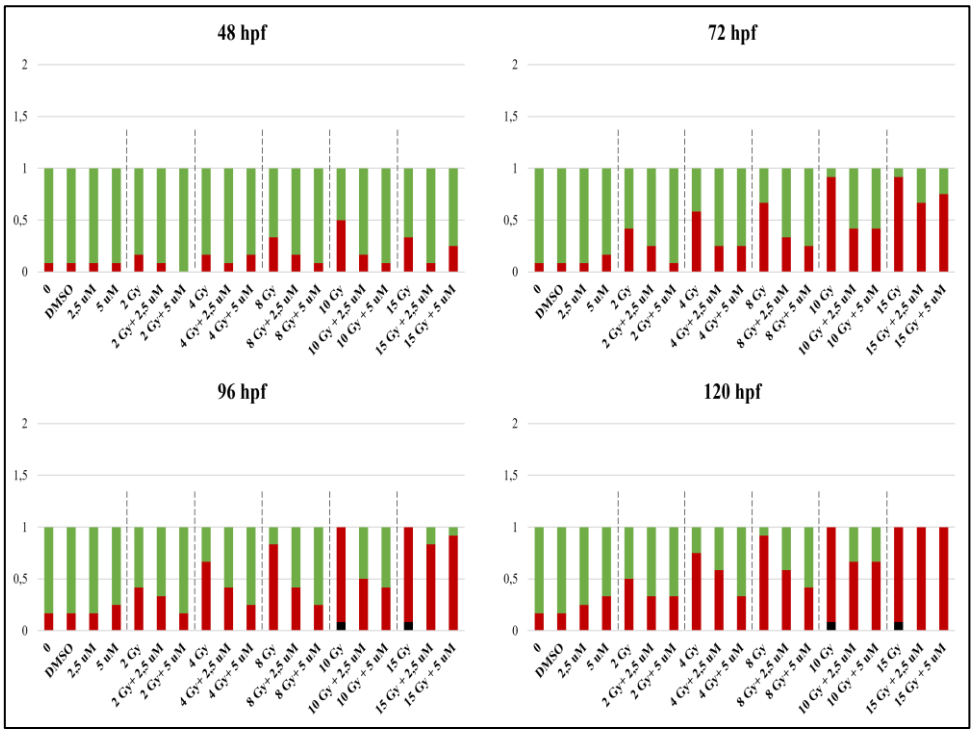

Fig. 33 *Normal (green bar), dead (black bar) and abnormal (red bar) embryos rates of developing zebrafish embryos exposed to 2, 4, 8, 10 and 15 Gy doses of proton beam with or without 2,5 and 5 µM curcumin concentrations. Data presented derived from 1 experiment.*

PE and SC started to be observed at 48 hpf for the higher doses (10 and 15 Gy), and at 72 hpf for the lower doses (≤ 8 Gy). Their incidence decreased in the presence of curcumin pre-treatment, from 72 up to 96 hpf, mainly with the 5 µM concentration. In detail, at 120 hpf, the incidence of SC was 80% and 100% in 10 and 15 Gy, respectively, *vs* 37% and 75% in the 5 µM pre-treated embryos with the same radiation doses. Similarly, at the same time point, the incidence of PE was 72% and 100% in 10 and 15 Gy, respectively, *vs* 50% and 41% in the 5 µM pre-treated embryos at the same radiation doses. Furthermore, despite the low incidence of these serious malformations at lower doses, the protective effect of curcumin was also confirmed, mainly with the 2.5 µM curcumin concentration (**Fig. 34**).

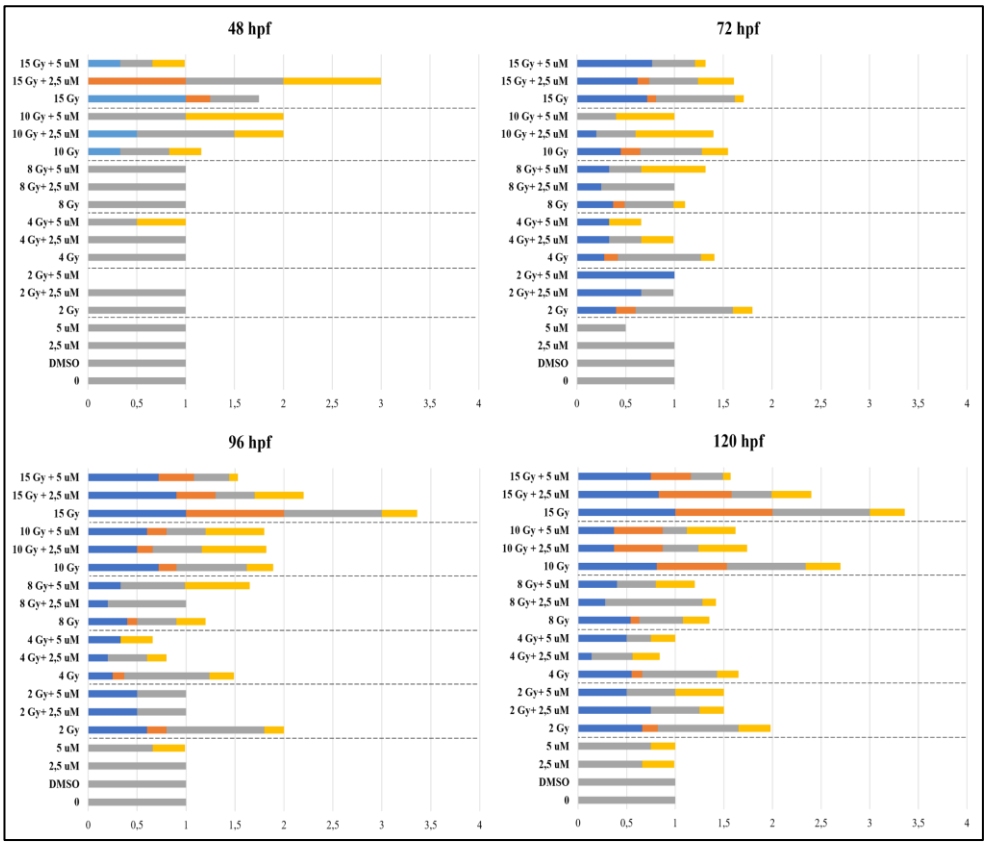

Fig. 34 *Distribution (%) of the main malformations observed in malformed developing zebrafish embryos exposed to a combination of curcumin pre-treatment with concentrations of 2.5 or 5 μM, followed by irradiation with 0, 2, 4, 8, 10 or 15 Gy of protons: SC (blue bar), PE (orange bar), YM (gray bar), PIGM (yellow bar). Data presented derived from 1 experiment.*

The evaluation of morphometric parameters at 72 and 96 hpf, such as body length, yolk sac diameter, eye length and head length, confirmed, at different extent, the protective effect exerted by curcumin pre-treatment for higher doses of radiation (10 and 15 Gy) (**Fig. 35 a, b**).

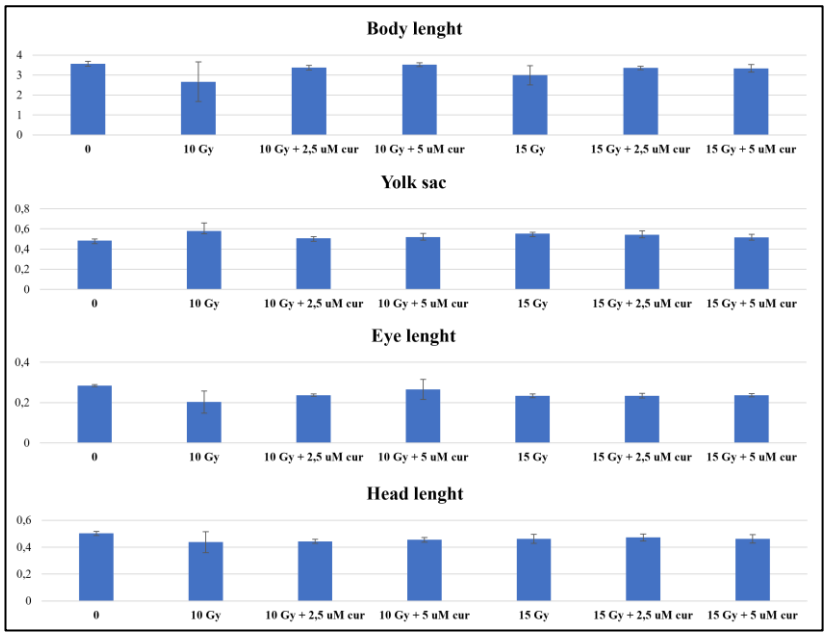

a.

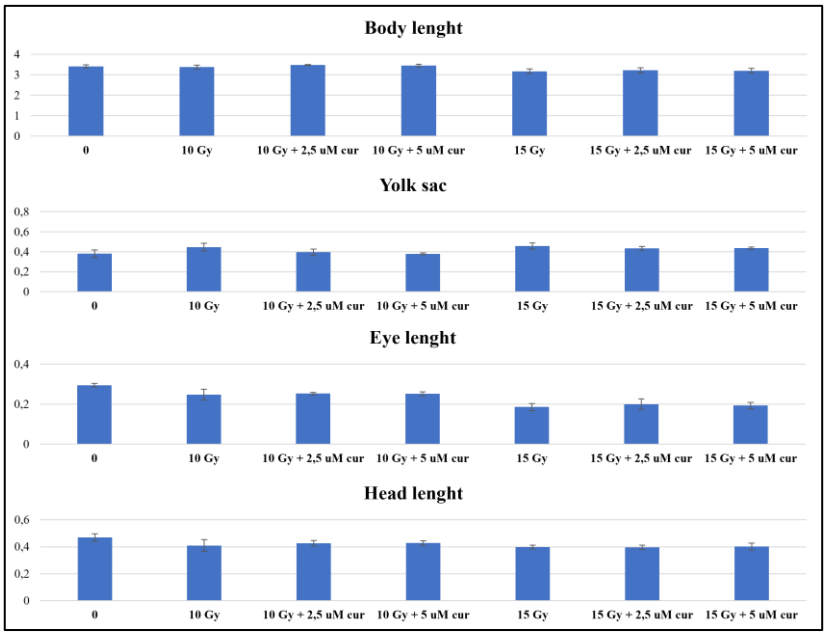

b.

Fig. 35 a, b *72 (**a**) and 96 (**b**) hpf measurement (mm) of morphological parameters (body length, yolk sac diameter, eye length and head length) after 10 and 15 Gy of proton treatment, with or without curcumin 2.5 and 5 µM pre-treatment. Data presented derived from 1 experiment. Error bar = ± SD.*

Even more interesting, the PE measurement, for the same treatments at the same time points, showed PE values of 0,15 and 0,12 mm at 72 hpf with 10 and 15 Gy, and 0,16 and 0,12 mm at 96 hpf with the same doses. Instead, in pre-treated embryos with 2.5 or 5 µM curcumin: the 72-hpf PE values were 0,12 and 0,1 mm with the dose of 10 Gy, and 0,1 and 0,13 mm with the dose of 15 Gy; the 96-hpf PE values were 0,11 mm with the dose of 10 Gy and

both the curcumin concentration, and 0,08 and 0,12 mm with the dose of 15 Gy (**Fig. 36**).

In the case of proton irradiation, the *Protection Rate* (PR) calculation showed the values reported in **Table n. 3**. Overall, the protection offered by curcumin is lower in combination with protons, than that offered in combination with photons, as above reported.

Moreover, based on the PE diameter values, even the *Relative Biological Effectiveness* (RBE) has been calculated for the 72 and 96 hpf embryos treated with 10 Gy, as described in materials and methods. The obtained values are reported in **Table n. 4**.

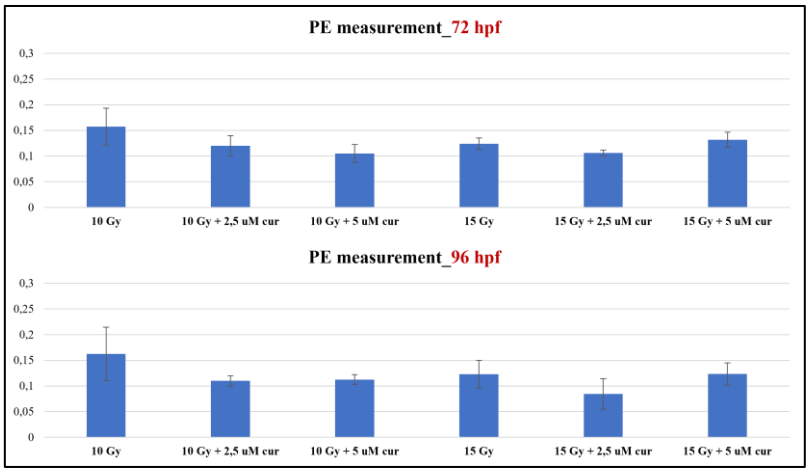

Fig. 36 *72 and 96 hpf measurement (mm) of PE measurement parameter after 10 and 15 Gy IR treatment, with curcumin pre-treatment, at both concentrations, or not. Data presented derived from 1 experiment. Error bar = ± SD.*

	72 hpf	**96 hpf**
10 Gy + 2,5 µM	20%	31%
10 Gy + 5 µM	33,33%	25%

Table n. 3 *Protection Rate (PR) values (%), for 10 Gy doses, with both concentration of curcumin, at 72 and 96 hpf, respectively.*

	72 hpf	**96 hpf**
10 Gy	0,93	1,25

Table n. 4 *RBE values calculated for the 72 and 96 hpf embryos treated with 10 Gy.*

The hatching rate analysis showed that the protons irradiation led to a delay of this phenomenon at 48 hpf of + 3,51% both for 2 and 4 Gy, + 2,50% for 8 Gy, + 2% for 10 Gy and +1,50% for 15 Gy, compared to untreated controls. Curcumin pre-treatment with both the concentrations led to a lower process delay at the same time point, with values similar to those of the control.

The manual evaluation of the heart-beating rate at 72 hpf, revealed a small decrease in the only irradiated embryos compared to controls, from 2 to 10 Gy (**Fig. 37**). Curcumin pre-treatment, at both concentrations, seems to exercise a protective role, bringing the values closer to those of the controls.

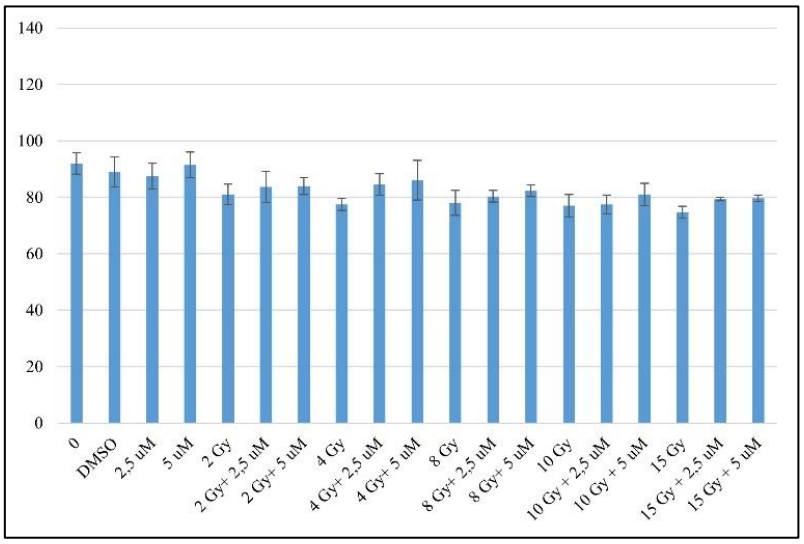

Fig. 37 *Heart rate values of 72 hpf embryos exposed to 2,5 and 5 μM curcumin concentrations and 2, 4, 8, 10 and 15 Gy of proton beam. Data presented derived from 1 experiment. Error bar = ± SD.*

DISCUSSIONS

Natural products are being increasingly valued by the scientific community, due to their potential application as an effective, safe, and cheap intervention, also in the context of personalized RT. Curcumin is a polyphenol derived from the plant *Curcuma longa*, and it exhibits strong antioxidant activity comparable to that of vitamins C and E. It was shown to be a potent ROS scavenger, including superoxide anion radicals, hydroxyl radicals and nitrogen dioxide radicals, which generally deteriorate the biomolecules such as protein, lipids, and nucleic acids especially DNA *(Dulbecco et al., 2013; Azmi et al., 2015).* In addition, the hydroxyphenyl chemical unit has been shown to be crucial to its anti-inflammatory activity *(Yallapu et al., 2014).*

The main aim of this research study was to evaluate the possible radioprotective effects of curcumin, using an *in vivo* approach on zebrafish embryos (*Danio rerio*). Specifically, embryos were subjected to single treatment with curcumin (2.5-10 μM) or radiation with X-rays or protons (2-15 Gy) and to combined treatments using 2 curcumin concentrations (2.5 e 5 μM) and 5 radiation doses (2, 4, 8, 10 e 15 Gy), using X-rays and protons. In particular, the irradiation with proton beam was just one first preliminary experiment.

The aim of a RT combined treatment should be based on the use of the lowest (effective) IR dose together with the lowest (no toxic) compound concentration, in order to obtain an additive or synergistic treatment to obtain the maximum efficacy on the tumor target without compromising surrounding healthy tissue.

Therefore, in order to evaluate the maximum possible toxicity caused by single treatments, a toxicological test was conducted using different curcumin dilutions in the absence of radiation and *viceversa*. Thus, a toxicology workflow has been defined to follow morphological alterations appearance on the treated embryos, as already described in material and methods.

The single treatment with curcumin was carried out by administering the molecule twice a day for five days, in order to cover eventual gaps due to the low half-life of the molecule during the entire period of embryos observation up to 120 hpf. Thus, this continuous administration could guarantee the

maximum toxic effects appearance induced by curcumin. In addition, due to the curcumin auto-florescence property, the fluorescence saturation and desaturation time has been evaluated in order to study the time of curcumin internalization and its permanence inside the embryos.

The treatment started at 6 hpf, when the maternal-to-zygotic transition of gene expression is almost complete, whereas the time of observation and analysis were concluded at 120 hpf, in order to avoid the necessity of animal experimentation authorization, according to European (2010/63/UE) and Italian (D. lgs. 26/2014) rules.

The effect of curcumin at different concentrations on zebrafish embryos and larvae had been previously studied by some researchers *(Chen et al., 2012; Rajagopal et al., 2017)*, and their findings showed a dose-dependent toxic effect of curcumin exposure. Our results showed that treatment concentrations of 7.5 and 10 μM were lethal, leading to 100% mortality at 72 and 48 hpf, respectively. In the lower range, the maximum mortality was 46% at 120 hpf with the concentration of 5 μM, with 47% of malformed embryos. The type and severity of deformities were observed to be concentration- and time of exposure - dependent. Among the observed malformations, treatment with 5 μM curcumin caused an early manifestation (24 hpf) of SC and PE with maximum percentages of 72 and 52%, respectively, at 120 hpf. The hatching rate evaluation at 48 hpf also showed that only the 5 μM curcumin treatment led to a phenomenon delay respect to the control. As already reported by *Oyemitan et al., 2017*, a significant increase in toxicity effect was mostly observed after hatching at 48 hpf, resulting into reduction in survival rate and physiological malformation from 72 hpf onwards. This result suggests that the accessibility of extract to embryo increases with the loss of the protective *chorion*. Indeed, previous experiment conducted by *Chen et al., 2010* showed continuous changes in the *chorion* protein profile of zebrafish embryos, as the age of development advances, leading to an increase in the widening of the *chorion* pore channel, permitting greater influx of external solutes.

The effect of the compound on the heartbeat rate of survived larvae at 72 hpf, treated with both 2.5 and 5 μM curcumin, showed no significant differences when compared with the control – with a very slight increase of 1%. A similar

result was previously reported *by Oyemitan et al., 2017*. The behavioural analysis showed a lower reactivity in response to an induced stimulus and a lower mobile capacity only for embryos treated with the 5 μM concentration, against a non-variation of the average speed maintained, confirming what has already been described in the literature (*Sachett et al., 2022*)

As already described by previous research groups (*Brunner et al., 2020*), embryo mortality as well as the rate of morphological aberrations increased with higher radiation dose, but decreased with advanced embryonic age and maturity (*Geiger et al., 2006*). Younger embryos, especially before *midblastula transition* (MBT), i.e. at the age < 24 hpf, were found to have not yet fully developed radiation damage repair proteins (*McAleer et al., 2005*), resulting in increased radiosensitivity and lower ability to repair the radio-induced damage. This strongly underlines that the zebrafish embryo model is highly suitable for radiation biology experiments from 24 hpf onwards, both to study radiation modifying agents as well as for comparative studies on the effects induced by different types of beams. Indeed, the increasing use of particle therapy and the emergence of innovative radiation methods raise the necessity of valid, reproducible preclinical data on the biological effects of radiations.

In our experiments, daily assessment of irradiated embryo until 120 hpf highlighted a very low mortality for embryos exposed from 2 to 15 Gy of X rays, than the untreated ones, as already described by *Szabò et al., 2016*. Indeed, in their experiment, the LD_{50} was 20 Gy on the 7th *day post irradiation* (dpi), for embryos irradiated with standard photon beam at 24 hpf. In addition, our experiments showed as IR inflicted malformations in a dose-dependent manner, in accordance with *Geiger et al. 2006*, with gross alterations from 8 Gy onwards, and an incidence of 50 and 82% in 15 Gy treated embryos at 48 and 120 hpf, respectively. Particularly, malformations strictly related to survival, such as SC and PE, prevailed for the higher doses (10-15 Gy) and appeared since 48 hpf, with values of 72 and 49%, respectively, at 120 hpf in 15 Gy irradiated embryos. As suggested by *Hwang et al., 2007*, such radiation-induced malformations in zebrafish model show similarity to those noted in mammals, as cataract formation and retinal degeneration/atrophy, microcephaly, spinal deformity, or pericardial effusion, indicating that the organization of cellular layers, in certain zebrafish body districts as well as in

those of humans, was noticeably perturbed by IR. These clinical manifestations overlap confirms the applicability of the embryo model for the development of innovative therapies, also considering that most zebrafish organs and tissues are fully formed within 48 hpf, with an almost total superimposition with human ones in terms of position and function.

Our hatching rate analysis showed that the IR treatment delayed this phenomenon at 48 hpf, in comparison to untreated controls, in a dose-dependent manner, as already observed by *Gan et al., 2019*. The permanence of the *chorion*, even in the following time points for the highest doses of radiation (8-15 Gy) highlights even more the correlation between increasing doses of IR and the toxicity in embryonic development.

Impaired heart rate, spontaneous movement, and swimming behaviour have also been reported following IR of developing zebrafish by other groups (*Li et al., 2018; Si et al., 2019; Zhou et al., 2015*). Similarly, our results showed a reduction in the heart rate of irradiated embryos, more for the higher doses and, despite a non-significant variation in the average speed maintained for the time unit and distance considered, a preference was highlighted in traveling short distances rather than the long ones. The two data could support each other, considering that a lower heart rate is mainly associated with small rather than large movements (*Gan et al., 2019*).

Thus, having identified the non-lethal and non-toxic concentration range of curcumin, and the effective dose range useful for the observation of the induced radiation damage, the objective was to investigate the effects of combined curcumin-radiation treatment induced in zebrafish early life stages by coupling responses obtained at phenotypic, circulatory and behavioural levels, as well as at the molecular level (gene expression of anti-oxidant or pro/anti-inflammatory genes) for experimental conditions of particular interest. Considering previous literature results, in our study we decided to investigate the combination of the lower curcumin concentration (2.5-5 μM) with increasing IR doses, reducing the curcumin administration only in the form of a 18-hour pre-treatment before the IR administration at 24 hpf.

As expected, considering the low rate of mortality given by radiation treatment alone in the selected dose range, irradiated embryos viability was not significantly affected by the 18 hours pre-treatment with 2.5 and 5 μM

curcumin, with respect to the controls. Interestingly, a pronounced protective effect was found in the percentage of malformed embryos after combined treatments using both the chosen curcumin concentrations, respect to the only irradiated embryos. Notably, this effect was visible in the 2-10 Gy range until the last day of observation (120 hpf), and it was greater for the higher curcumin concentration (5 μM), with a recovery of 21 and 11% for doses of 8 and 10 Gy, respectively. On the other hand, the dose of 15 Gy proved to be a *threshold* dose, as a slight protective effect of curcumin was observed only up to 96 hpf (4%), probably due to the greater, irreparable severity of the radiation-induced damage. These results are in line with what has been observed by *Szabó et al., 2018*, in which a relevant deterioration occurred during day 4 post IR and increased thereafter at 15-20 Gy radiation dose. The protective effect of curcumin, in detail, was manifested in the reduced incidence of specific malformations, with a SC recovery of 15% and 14% for doses of 10 and 15 Gy, at 96 hpf, and a PE recovery of 23 % and 22% for the same doses at the same time point, respectively. Therefore, the greatest protection, in percentage terms, seems to be exerted on the malformation closely related to the embryos and larvae survival, i.e. PE. This acquires greater value considering that severe PE could led to a circulatory collapse in developing zebrafish and to the end-stage heart failure as described by *Chen, 2013*. Furthermore, the curcumin protection is exerted not only in terms of incidence of PE occurrence, but also in terms of phenotype severity, which is less extensive in the pre-treated embryos *vs* the only irradiated ones.

The analysis of morphometric parameters at 72 and 96 hpf showed a lesser severity of all the other malformations under examination, such as body length, yolk sac diameter, eye length and head length, although the more interesting recovery was just in the PE diameter.

Thus, in our study, we also quantified the entity of curcumin radioprotective ability, by means of the evaluation of a *Protection Rate* (PR) parameter, which showed that the pre-treatment with the lower concentration of curcumin (2.5 μM) led to an higher reduction in the PE diameter than the 5 μM concentration *vs* irradiation alone, with values of 39,28 and 50% at 72 and 96 hpf for 10 Gy irradiated embryos, respectively. Therefore, the lower concentration of curcumin seems to act more effectively in reducing the PE diameter. As a confirmation of this protection against the heart district, the

evaluation of the heart-beating rate at 72 hpf revealed as curcumin pre-treatment, at both concentrations - but again little better with the lower one - seems to exercise a protective role, bringing the heartbeat values closer to those of the controls for the 2-10 Gy dose range. Curiously, embryos treated with dose of 15 Gy with or without curcumin suffered of increased heartbeat, as the PE volume is more pronounced than for doses ≤ 10 Gy, so the heart try to compensate with an increased heart frequency. Also in this case, albeit not significantly, the lower concentration of curcumin seems to act by lowering the values back to those of the control.

IR is an important source of exogenous ROS, which exhaust the tissue's antioxidant system, stimulates the production of more ROS to form a cascade of amplified inflammatory responses and, ultimately, leads to cell death (*Dong et al., 2020*). Thus, oxidative stress is a central pathogenic mechanism mediating radiation damage, suggesting that curcumin protection could be associated with an enhanced antioxidant capacity. Consistent with this notion, we observed that the gene expression of some crucial antioxidant enzymes was reduced by irradiation compared to the control group, whereas their levels were reported close to those of controls in the pre-treated embryos. This trend has been observed by other researchers, testing other radioprotective molecules (*Gan et al., 2019*). As described in the literature, in response to external stimuli, such as IRs, transcription factors of the FOXO family regulate the expression of genes involved in cell cycle arrest, survival processes and, above all, in the response to oxidative stress (*Greer and Brunet, 2005*). Among them we highlighted *sod1*, *sod2*, *gpx*, *cat*, *gstp* and *xdh*, responsible for the production of the homonymous antioxidant enzymes, which give to the cells the ability to resist to the ROS excess by preventing the triggering of the apoptotic process (*Nho and Hergert, 2014*). The importance of these enzymes does not lie only in their role of detoxification, but also in the fact that their activities are synergic and coordinated. There are three types of SOD: *cytosol Cu–Zn-SOD* (SOD1), *manganese-dependent mitochondrial enzyme Mn-SOD*, (SOD2) and *extracellular Cu-Zincase EC-SOD* (SOD3). O_2- formed in mitochondria is degraded to H_2O_2 by SOD1 in the mitochondrial membrane gap and by SOD2 in the mitochondrial matrix (*Wang et al, 2016; Cai et al., 2017*). GPX (1-4) in the mitochondrial matrix eliminates H_2O_2, while uncharged H_2O_2 passes through the mitochondrial

membrane and is cleared by cytoplasmic SOD1 or CAT. SOD1 is also essential for Caspase-1 activation and regulation of the oxidation and glutathionylation of specific cysteine residues. CAT splits H_2O_2 into H_2O and O_2, and it can reduce inflammation *in vitro*, inhibiting caspase-1 activity and IL-1 β production and maturation (*Cai et al., 2017*). GPX converts *tripeptide glutathione* (GSH), which is composed of glutamate, cysteine and glycine, into *oxidized glutathione* (GSSG); H_2O_2 is reduced to H_2O in this process, and *lipid hydrogen peroxide* (ROOH) is reduced to the corresponding stable alcohol. The GPX reaction is coupled with *glutathione reductase* (GSR), which maintains *reduced glutathione* (GSH) levels (*Li et al., 2015*). Among the cellular functions attributed to GSTs there are those of ligand binding and xenobiotic detoxification (*Tew, 1994*), indeed, reduced glutathione (GSH) binds to the 'G' site of GSTp (and other GST isozymes) and plays an important role in detoxification of reactive oxygen species (ROS) and the maintenance of the cellular redox state (*Sato et al., 1989*). The *xanthine oxidoreductase* (XOD) system, which consists of *xanthine dehydrogenase* (XDH) and *xanthine oxidase* (XO), is one of the major sources of free radicals in biological systems. The XOD system is predominantly present in the normal tissues as XDH. In damaged tissues, XDH is converted into XO, the form that generates free radicals. IR has been shown to convert XDH into XO, contributing to cell damage. The radiation-induced depletion of GSH and other thiols, essential for XDH maintaining in its reduced form *in vivo*, may also contribute to the conversion of XDH into XO, which has been reported to be irreversible (*Srivastava et al., 2002*).

Overall, in our study, the analysis of gene expression levels of these enzymes, involved in the detoxification pathway or hydroxyl radical and superoxide anion scavenging activity, showed their deacrease in the 10 Gy irradiated embryos, whereas their levels were close to those of controls in embryos subjected to combined treatment (10 Gy/5 μM curcumin) or in embryos treated with curcumin as single treatment. Thus, interestingly, curcumin seems to be able to revert the downregulation of the gene expression of *sod1*, *sod2*, *gpx1a/4a*, *cat*, *gstp/1a* and *xdh*, restoring the detoxification capacity of cells subjected to IR treatment.

In addition, another interesting result of our study is the observation of a similar trend also for the transcription factor STAT3, with increased

expression levels in the combined-treated embryos respect to the irradiated alone, both normalised to the controls. STAT3 can be activated by various growth factors and have protective role against IR damage, upregulating genes that are antioxidant, antiapoptotic, pro-angiogenic and pro-inflammatory, even if suppressing anti-inflammatory and anti-fibrotic genes. It is also recognized to have other non-genomic roles targeting mitochondrial function and autophagy (*Yu et al., 2009*). Interestingly, a group of researchers showed that CAT treatment *in vitro* protects normal cells against radiation-induced DNA damage and apoptosis via promoting STAT3 activation, increasing the expression of anti-apoptotic proteins such as BCL-2 and Survivin (*Gu et al., 2007*). In addition, the radioprotective effect of CAT, associated with increased STAT3 activation and elevated Survivin expression, was also confirmed by the experimental inhibition of STAT3, that abolished the protective activity of CAT in cells. These novel observations suggest that CAT may inhibit IR-induced oxidative stress, DNA damage, and apoptosis, at least in part, through activating the STAT3 signalling pathway. In support of this idea, it has been recently shown that STAT3 can bind to and affect the enzymatic activities of several subunit complexes of the mitochondrial electron-transport chain, thus demonstrating a new and noncanonical role for STAT3 in mitochondrial function (*Wegrzyn et al., 2009; Tammineni et al., 2013*).

In addition, among genes involved in energy metabolism, we investigated the possible variation in *ldha* expression levels, as it codes for an enzyme capable of catalyzing the reversible conversion of pyruvate into lactate, simultaneously with the oxidation/reduction of a NADH/NAD+ molecule (*Forkasiewicz et al., 2020*). The isoform *a* mainly catalyzes the reaction from pyruvate to lactate by a reaction that oxidizes a NADH molecule (*Wang et al., 2012*). It is one of the main enzymes involved in anaerobic glycolysis, and its expression can not only determine the energy metabolic pathway mainly used by the cell but can also affect the amount of intracellular ROS (*Wang et al., 2012*). It has been shown that cells with a high proliferative rate, such as cancer, stem and progenitor cells, have overexpression of LDHA and a lower amount of ROS compared to quiescent cells that metabolize glucose through the oxidative phosphorylation chain (*Wang et al., 2012; Donmez et al., 2013*). The activation of *ldha* expression and the presumable consequent formation

of the enzyme reduces the production of intracellular ROS derived from glucose oxidation (*Valvona et al., 2015*). This evidence, associated with a significant increase in its expression levels observed in pretreated embryos compared to irradiated ones (2.07 *vs* 0.33 *fold-change*), further confirms the hypothetical protective power of curcumin against ROS. Furthermore, the LDHA enzyme is also able to influence the NAD+/NADH *ratio* by increasing it. In this way, the catalytic activity of *Sirtuins* (SIRT1-6) is stimulated and, consequently, this could favour a further antioxidant effect (*Vettraino et al., 2013*). Given the significant involvement of ROS in IR-induced normal tissue toxicity, damage and death, the results up to now described permit to hypothesize that curcumin protect by IR induced toxicity, by modulating the gene expression of antioxidant and detoxifying enzymes, thus promoting cell survival.

We also investigated the inflammatory profiles of treated embryos, through the gene expression analysis of the cytokines *il-1β*, *il-6*, *tnf-α* and *il-10*. Once again, they showed a similar trend, with expression levels lower than 1 (referred to untreated embryos) in any treatment studied. This could be explained by the fact that in the larvae, at the time of hatching (48-72 hpf), the immune system is still developing and not all of the structures and functions are mature (*Ellis, 1988; Tatner, 1996*). After fertilization, larvae survive with only the innate immune responses because adaptive immune system, both cell-mediated and humoral immunity, is non-functional during the early larval stages and becomes fully competent after both lymphoid organs and cells mature several weeks (from 1 to 15) after hatching (*Lam et al., 2002*). However, interestingly, the combined treated embryos showed higher expression level of these four cytokines compared to that of solely IR and curcumin treated embryos. This could be related, as described before, by the STATs role in inflammation and immunity. The *stat3* increase in combined-treated embryos, could motivate the *trend* observed for these four cytokines, considering the leading role of STAT3 in the expression regulation of cytokines, chemokines, and other mediators, such as IL-6, IL-1β or IL-10, macrophage colony-stimulating factor, prostaglandins, and cyclo-oxygenase 2 (*Yu et al., 2009*). Surely, it would be interesting to pay attention to these parameters in time points later than 48 hpf.

Therefore, based on what it has been observed and highlighted, curcumin radioprotection is activated after the IR insult at molecular, cellular, tissue and organism levels.

Furthermore, we also tested the curcumin pre-treatment in combination with a proton beam irradiation, placing the embryos in the mid-SOBP position, in order to verify if the entity of curcumin radioprotection by IR-induced toxicity is same to that observed with photon conventional irradiation. Indeed, the RBE of protons is known to be close to 1.1, thus it is expected to be little bit more effective and toxic.

Proton irradiation as single treatment led to a very low mortality for embryos exposed from 2 to 15 Gy, compared to the untreated ones, with a maximum death of 9% for the higher doses (10 and 15 Gy) at 120 hpf. Curcumin pre-treatment, at both concentrations, led to 0% dead embryos at the same time point and with the same doses. As described by *Szabò et al., 2018* the survival of 24 hpf zebrafish embryos was not reduced significantly by doses up to 15 Gy of protons (and photons) at the entrance of plateau, and up to 10 Gy at mid-SOBP, respectively. Interestingly, in their experiments the number of surviving embryos significantly declines at higher doses, as for protons the delivery of 30 Gy resulted in a 50% survival rate (LD_{50}) already at the 4^{th} dpi.

In our experiment comparing proton *vs* photon beam irradiation as single treatments, in proton-treated embryos, the highest percentages of malformed embryos range from 75% with the 4 Gy dose to 91% with the 10 and 15 Gy doses at 120 hpf, whereas lower range of malformed embryos were observed after photons irradiation at the same timepoint: 49,9% (4 Gy) to 87,4% (10 and 15 Gy) (**Table n. 5**). This comparison confirms that, at the isodose, the damage inflicted by protons is greater than that inflicted by photons.

The combination of proton irradiation with curcumin pre-treatment also reduced the percentages of malformed embryos at 120 hpf, in a concentration-dependent manner. Indeed, with the 5 µM curcumin pre-treatment, the percentage of malformed embryos at 120 hpf were 33% and 66% at 4 and 10 Gy, respectively, *vs* 35% e 66% observed, at the same time point and for the same doses, in curcumin pre-treated embryos with photon beam. The **Table n. 5** show how curcumin pre-treatment produces a major gain in malformation

percentage recovery in combination with protons than with photon irradiation.

	4 Gy	*4 Gy + 5 μM*	10 Gy	*10 Gy + 5 μM*
Photons	49,9%	35%	87,4%	66%
Protons	75%	33%	91%	66%

Table n. 5 *Malformation percentage induced by photons or protons at 4 and 10 Gy doses, in combination or not with 5 μM curcumin, at 120 hpf.*

Instead, using 15 Gy of photon or proton beams, the dose effect seems to prevail over the radioprotective effect exerted by curcumin. Indeed, at 96 hpf the percentage of malformed embryos are 91,6% with photons single treatment *vs* 87,4% in combination with 5 μM curcumin; whereas, they are 91,6% both with protons single treatment or in combination with 5 μM curcumin. Moreover, at 120 hpf no gain is observed by the combination of curcumin with IR.

Thus, in our study the 10 Gy could be considered a *threshold dose* in order to benefit of radioprotective effects offered by curcumin. Similar results were previously found by the group of *McAleer et al., (2005)* with another compound.

In proton irradiation, the PE and SC started to be observed at 48 hpf for the higher doses (10 and 15 Gy), and at 72 hpf for the lower doses (≤ 8 Gy). Their incidence decreased in the presence of curcumin pre-treatment, from 72 up to 96 hpf, mainly with the 5 μM concentration. In detail, at 120 hpf the SC incidence was 80% and 100% in 10 and 15 Gy (*vs* 61% and 85% observed with photons), respectively. Its incidence decreased in the 5 μM pre-treated embryos with the same radiation doses, being 37% and 75% with protons (*vs* 45 and 85% with photons). Thus, the SC incidence is higher with protons than with photons, and 5 μM curcumin would seem to offer a higher gain of protection with protons than with photons. This effect is also visible with the dose of 15 Gy, as the SC percentage decrease from 100% to 75 % in the combined treated embryos.

Similarly, at the same time point, the incidence of PE after proton irradiation was 72% and 100% (*vs* 66 and 100% with photons) in 10 and 15 Gy, respectively. Its incidence decreased in the 5 μM pre-treated embryos with

the same radiation doses, being 50% and 41% with protons (*vs* 30 and 95% with photons). Thus, also the PE incidence confirm the higher effect of curcumin on protons than photon irradiated embryos.

However, we also investigated the curcumin radioprotection in terms of malformation severity. The evaluation of morphometric parameters at 72 and 96 hpf, such as body length, yolk sac diameter, eye length and head length, confirmed, at different extent, the protective effect exerted by curcumin pre-treatment for higher doses of radiation (10 and 15 Gy).

In particular, even for proton irradiation, we focused our attention on the PE diameter, as main alteration that could easily outcome in death. Thus, we measured the PE diameter average for all the treatment configurations and calculated the *Protection Rate* (PR) offered by curcumin, as already described in materials and methods. As it can be easily observed, the severity of PE in terms of its diameter is similar at the isodose of 10 Gy in photons (0,14 mm) and proton (0,15 mm) treated embryos at 72 hpf and at 96 hpf (0,16 mm for both the beams). However, the PE improvement offered by curcumin is major in combination with photons than with protons, as a greater diameter reduction is appreciable in the first combination. In particular, as shown in **Tables n. 2-3**, at 10 Gy the *Protection Rate* offered by 2.5 and 5 μM curcumin is higher in photon treated embryos for both the time points of 72 hpf (39,28% and 28,57%) and 96 hpf (50% and 25%), *vs* proton treated embryos at the same time points (20% and 33,3% at 72 hpf, while 31,25% at 96 hpf for both the curcumin concentration). Particularly, a major effectiveness is offered by the lower curcumin concentration. Based on the main role of curcumin in cell detoxification, these results suggest that the PE malformation could be more affected by ROS production (*Razaghi et al., 2018*) in photon than in proton beam irradiation, thus supporting the idea of the higher indirect damage due to water radiolysis generated by photons, than that produced by proton and, in general by hadrons.

The hatching rate analysis showed that the protons irradiation led to a delay of this phenomenon at 48 hpf compared to untreated controls, as already reported by *Hu et al., 2016* and *Li et al., 2018*. Like with photons, even for proton irradiation the curcumin pre-treatment with both the concentrations led to a lower delay process at the same time point, with values similar to

those of the control. The manual evaluation of the heart-beating rate at 72 hpf, revealed a small decrease in the only irradiated embryos compared to controls, from 2 to 10 Gy and, even in this case, curcumin pre-treatment at both concentrations seems to exercise a protective role, bringing the values closer to those of the controls.

Finally, based on the PE diameter values we calculated the RBE of photons respect to protons at the isodose of 10 Gy, in order to compare just the beams biological effectiveness. The RBE is known to be variable and influenced by different factors such as tissue type, biological endpoint, treatment regimen, ion type (*Lühr et al., 2017*). In order to overcome the uncertainties of the *in vitro* experiments, *in vivo* systems (clinically more relevant) have been introduced in radiation research providing important data on the dose dependent reactions of a complex organism. Respect to rodents, the development of a less vulnerable, and less expensive novel *in vivo* vertebrate model, which fulfills the requirements drawn up by *Hall (1979)* to be a "convenient, portable and reproducible" biological system for inter-comparison, is essential for studies on emerging radiation modalities. However, a substantial difference exists in the calculation of the RBE *in vitro* and *in vivo*. In fact, for cultured cells, the calculation of the RBE is consolidated and based on the dose's ratio between photons and protons, necessary to obtain the isoeffect in terms of the same survival values, obtained from two LQ model dose response curves (*Savoca et al., 2020*). In the case of *in vivo* RBE calculation, it cannot be possible to evaluate it by doses ratio at a certain survival isoeffect, as survival values are discrete because they are experimentally generated, not being possible to obtain them from a LQ model curve.

Therefore, some examples of RBE calculation are reported in the literature on zebrafish model.

In particular, the RBE definition of high LET beams relied on two quantitative endpoints, as survival or morphometric parameters' ratios at the isodose. Considering the survival parameter, other research groups have found RBE values in the range of 0,96 – 1,2 at 4 dpi after 20 Gy of plateau and mid-SOBP protons (*Urano et al., 1984; Uzawa et al., 2007; Saager et al., 2018*). Instead, considering morphometric parameters of malformations

at 4 dpf, the RBE was previously estimated for SC and YM, but not for PE, although it is observed as an acute reaction in all embryos, closely related to survival in the embryonic stages (*Brunner et al., 2020)*. Then, we decided to consider the PE diameter at the isodose of 10 Gy for the RBE calculation, finding the values of 0,93 and 1 at 72 hpf and 96 hpf respectively, thus confirming a similar biological efficacy between the two beams. However, considering that in this study the proton irradiation has been performed as single experiment, we should consider these results as preliminary and further replicates are needed to confirm the data obtained.

CONCLUSION AND FINDINGS

1) This is an unprecedented radiobiological study focusing the role of curcumin as radioprotector on zebrafish model;
2) Curcumin has proved to be a powerful radioprotector *in vivo*;
3) Curcumin pre-treatment reduced the overall incidence of malformed embryos and the percentage of single malformations with both the beam types;
4) Curcumin has proved to be more efficient in reducing the incidence of malformations induced by protons, compared to photons, also in reducing the PE diameter, probably due to a major ROS contribution, induced by photons, to the PE severity;
5) The radioprotective effect of curcumin most likely depends on the antioxidant activity of curcumin.

FUNDING

The project was funded by a *PhD grant from the University of Palermo*, by the "*PBCT Proton Boron Capture Therapy" PRIN 2017 Project - grant Prot. 2017XKWWK9* and by the *"FLASH Radiotherapy with hIgh Dose-rate particle beAms (FRIDA)" Project – INFN CSN5 Call 2021*.

APPENDIX A

List of primers used for q-PCR

Gene	Sequences (5'-3') Forward (Fw) and Reverse (Rw)	Length (bp)	Annealing T (C°)
cat	F: ATGAAGCCGAGAGAGAGCGT R: TCAGCGTTGTGTTTATCCAGG	20 21	62
sod1	F: AAGAAGCCAGTGAAGGTGACT R: CGTGTCTCACACTATCGGTTG	21 21	62
sod2	F: TGTGCTAACCAAGACCCTTTG R: AACGCTCGCTGACATTCTCC	21 20	62
gpx1a	F: GCACAACAGTCAGGGATTACA R: AGCCATTTCCAGGACGGAC	21 19	62
gpx4a	F: TTCACAGCCACAGATATAGATG R: GAAAGCCAGGATGCGTAAACC	22 21	62
xdh	F: ATAGTGATGGATGTGGGCAAG R: TAACCGTCAGGAGAGTAGCG	21 20	62
gstp	F: TCGCAGTCAAAGGCAGATGTG R: GAAACAGCACCAGGTCACCAT	21 21	62
gstp1a	F: TCTACCAGGAATATGAGACCG R: ACCTTCAGATTCAGCAGCAGA	21 21	62
ldha	F: GTTGGAATGGTTGGAATGGCT R: CTTGTGCGTCTTGAGAAACAG	21 21	62
stat3	F: GGCTGGACAACATTATTGACC R: GGAGGCTTTGGACTCAGGAT	21 20	62
il-1β	F: CCCTGAACAGAATGAAGCACA R: TGTAAGACGGCACTGAATCCA	21 21	62
il-6	F: CAAGATGCCATCCGCTCAGA R: CCTGAACTTCGTCTCCCAGATA	20 22	62
il-10	F: TTCAGGAACTCAAGCGGGATA R: GTACCTAAAGAGCAAATCAAGC	21 22	62
tnf-α	F: TCTGCTTCACGCTCCATAAGA R: GTCATCTCTCCAGTCTAAGGT	21 21	62
rpl13	F: AGGTGTGAGGGTATCAACATC R: TTGGTTTTGTGTGGAAGCATAC	21 22	62

APPENDIX B

Dead, abnormal and normal embryos rates, observed at 96 and 120 hpf, of developing malformed zebrafish embryos exposed to a combination of curcumin pre-treatment with concentrations of 2.5 or 5 μM, followed by irradiation with 0, 2, 4, 8, 10 or 15 Gy of X-rays.

96 hpf	Dead	Abnormal	Normal
0	*0,1*	*0,027*	*0,87*
DMSO	*0,1*	*0,05*	*0,84*
2,5 μM cur	*0,1*	*0,11*	*0,78*
5 μM cur	*0,19*	*0,11*	*0,68*
2 Gy	*0,11*	*0,36*	*0,52*
2 Gy + 2,5 μM cur	*0,05*	*0,27*	*0,66*
2 Gy + 5 μM cur	*0,11*	*0,19*	*0,69*
4 Gy	*0,05*	*0,44*	*0,50*
4 Gy + 2,5 μM cur	*0,11*	*0,30*	*0,58*
4 Gy + 5 μM cur	*0,16*	*0,36*	*0,47*
8 Gy	*0,13*	*0,49*	*0,36*
8 Gy + 2,5 μM cur	*0,11*	*0,38*	*0,5*
8 Gy + 5 μM cur	*0,03*	*0,47*	*0,5*
10 Gy	*0*	*0,87*	*0,13*
10 Gy + 2,5 μM cur	*0,05*	*0,58*	*0,37*
10 Gy + 5 μM cur	*0,05*	*0,45*	*0,50*
15 Gy	*0,05*	*0,91*	*0,04*
15 Gy + 2,5 μM cur	*0*	*0,79*	*0,21*
15 Gy + 5 μM cur	*0*	*0,87*	*0,13*

120 hpf	Dead	Abnormal	Normal
0	*0,1*	*0,03*	*0,87*
DMSO	*0,1*	*0,09*	*0,81*
2,5 μM cur	*0,12*	*0,14*	*0,72*
5 μM cur	*0,19*	*0,14*	*0,66*
2 Gy	*0,13*	*0,41*	*0,44*
2 Gy + 2,5 μM cur	*0,07*	*0,27*	*0,66*
2 Gy + 5 μM cur	*0,11*	*0,22*	*0,66*
4 Gy	*0,05*	*0,49*	*0,44*
4 Gy + 2,5 μM cur	*0,11*	*0,36*	*0,52*
4 Gy + 5 μM cur	*0,16*	*0,35*	*0,47*
8 Gy	*0,13*	*0,63*	*0,22*
8 Gy + 2,5 μM cur	*0,11*	*0,52*	*0,36*
8 Gy + 5 μM cur	*0,04*	*0,52*	*0,44*
10 Gy	*0,05*	*0,87*	*0,08*
10 Gy + 2,5 μM cur	*0,06*	*0,74*	*0,20*
10 Gy + 5 μM cur	*0,05*	*0,66*	*0,29*
15 Gy	*0,12*	*0,87*	*0,01*
15 Gy + 2,5 μM cur	*0,05*	*0,95*	*0*
15 Gy + 5 μM cur	*0,08*	*0,91*	*0,01*

APPENDIX B.1

Distribution (%) of SC and PE, observed at 96 and 120 hpf, in developing malformed zebrafish embryos exposed to a combination of curcumin pre-treatment with concentrations of 2.5 or 5 μM, followed by irradiation with 0, 2, 4, 8, 10 or 15 Gy of X rays.

96 hpf	**SC**	**PE**
0	*0*	*0*
DMSO	*0,16*	*0*
2,5 μM cur	*0,5*	*0,16*
5 μM cur	*0,33*	*0*
2 Gy	*0,29*	*0,04*
2 Gy + 2,5 μM cur	*0*	*0*
2 Gy + 5 μM cur	*0,33*	*0*
4 Gy	*0,16*	*0,11*
4 Gy + 2,5 μM cur	*0,21*	*0*
4 Gy + 5 μM cur	*0,08*	*0*
8 Gy	*0,34*	*0,14*
8 Gy + 2,5 μM cur	*0,2*	*0,06*
8 Gy + 5 μM cur	*0,12*	*0*
10 Gy	*0,55*	*0,48*
10 Gy + 2,5 μM cur	*0,32*	*0,45*
10 Gy + 5 μM cur	*0,4*	*0,25*
15 Gy	*0,56*	*0,7*
15 Gy + 2,5 μM cur	*0,44*	*0,48*
15 Gy + 5 μM cur	*0,42*	*0,48*

120 hpf	**SC**	**PE**
0	*0*	*0*
DMSO	*0,11*	*0*
2,5 μM cur	*0,5*	*0*
5 μM cur	*0,33*	*0*
2 Gy	*0,31*	*0,04*
2 Gy + 2,5 μM cur	*0*	*0*
2 Gy + 5 μM cur	*0,33*	*0*
4 Gy	*0,14*	*0,09*
4 Gy + 2,5 μM cur	*0,21*	*0*
4 Gy + 5 μM cur	*0,08*	*0*
8 Gy	*0,39*	*0,2*
8 Gy + 2,5 μM cur	*0,22*	*0,04*
8 Gy + 5 μM cur	*0,23*	*0,04*
10 Gy	*0,61*	*0,66*
10 Gy + 2,5 μM cur	*0,34*	*0,5*
10 Gy + 5 μM cur	*0,45*	*0,3*
15 Gy	*0,85*	*1*
15 Gy + 2,5 μM cur	*0,59*	*0,91*
15 Gy + 5 μM cur	*0,86*	*0,95*

ABBREVIATIONS

BC *Breast Cancer*

DCFH-DA *2,7-Dichlorofluoroscin Diacetate*

DMSO *Dimethyl Sulfoxide*

dpf *days post fertilization*

dpi *days post irradiation*

DSBs *Double Strand Breaks*

hpf *hours post fertilization*

HR *Hatching Rate*

IGRT *Image-Guided RT*

IMRT *Intensity-Modulated RT*

IR *Ionizing Radiation*

Lardist *Large Distance*

LET *Linear Energy Transfer*

LNT *Linear and No-Threshold*

LQ *Linear Quadratic*

NTC *Non-Template Control*

NTCP *Normal Tissue Complication Probability*

PE *Pericardial Edema*

PIGM *Pigmentation*

PK/PD *Pharmacokinetic/Pharmacodynamic*

PMMA *Polymethyl Methacrylate*

PR *Protection Rate*

PT *Proton Therapy*

RBE *Relative Biological Effectiveness*

ROS *Reactive Oxygen Species*

RT *Radiotherapy*

rt *room temperature*

SC *Spinal Curve*

SD *Standard Deviation*

SLN Solid Lipid Nanoparticle

Smlsdist *Small Distance*

Smlspeed *Small Speed*

SOBP *Spread-Out Bragg Peak*

SSBs *Single Strand Breaks*

TCP *Tumor Control Probability*

TFs *Transcription Factor*

YM *Yolk Malabsorption*

zPDX *zebrafish patient-derived xenograft*

REFERENCES

Abdelkader TS, Chang SN, Kim TH, Song J, Kim DS, Park JH. Exposure time to caffeine affects heartbeat and cell damage-related gene expression of zebrafish Danio rerio embryos at early developmental stages. *J Appl Toxicol. 2013 Nov;33(11):1277-83*.

Abraham SK, Sarma L, Kesavan PC. Protective effects of chlorogenic acid, curcumin and beta-carotene against gamma-radiation-induced *in vivo* chromosomal damage. *Mutat Res. 1993;303(3):109–112*.

Aggarwal BB, Deb L, Prasad S. Curcumin differs from tetrahydrocurcumin for molecular targets, signaling pathways and cellular responses. *Molecules. 2014;20:185–205*.

Amalraj A, Pius A, Gopi S, Gopi S. Biological activities of curcuminoids, other biomolecules from turmeric and their derivatives - A review. *J Tradit Complement Med. 2016 Jun 15;7(2):205-233*.

Arjmand B, Tayanloo-Beik A, Foroughi Heravani N, Alaei S, Payab M, Alavi-Moghadam S, Goodarzi P, Gholami M, Larijani B. Zebrafish for Personalized Regenerative Medicine; A More Predictive Humanized Model of Endocrine Disease. *Front Endocrinol (Lausanne). 2020 Jul 17;11:396*.

Ashrafizadeh M, Ahmadi Z, Mohammadinejad R, Farkhondeh T and Samarghandian S. Curcumin Activates the Nrf2 Pathway and Induces Cellular Protection Against Oxidative Injury. *Current Molecular Medicine 2020, 20, 116-133*.

Azmi L, Ojha SK, and Rao CV. Curcumin: Boon for Human Being. *World J. Pharm. Pharm. Sci., vol. 4, no. 6, pp. 239–249, 2015*.

Baeten JT, de Jong JLO. Genetic Models of Leukemia in Zebrafish. *Front Cell Dev Biol. 2018 Sep 20;6:115*.

Banaz-Yasar F, Lennartz K, Winterhager E, Gellhaus A. Radiation-induced bystander effects in malignant trophoblast cells are independent from gap junctional communication. *J. Cell. Biochem. 2007;103:149–161*.

Baskar R, Dai J, Wenlong N, Yeo R, Yeoh KW. Biological response of cancer cells to radiation treatment. *Front. Mol. Biosci. 2014;1:24*.

Bernstein EF, Sullivan FJ, Mitchell JB, Salomon GD, Glatstein E. Biology of chronic radiation effect on tissues and wound healing. *Clin Plast Surg 1993;20:435–53*.

Bertoncello KT, Aguiar GPS, Oliveira JV, Siebel AM. Micronization potentiates curcumin's anti-seizure effect and brings an important advance in epilepsy treatment. *Sci Rep. 2018 Feb 8;8(1):2645*.

Blank KR, Rudoltz MS, Kao GD, Muschel RJ, McKenna WG. The molecular regulation of apoptosis and implications for radiation oncology. *Int J Radiat Biol. 1997 May;71(5):455-66.*

Boerma M, Davis CM, Jackson IL, Schaue D, Williams JP. All for one, though not one for all: team players in normal tissue radiobiology. *Int J Radiat Biol. 2022;98(3):346-366.*

Brannen KC, Panzica-Kelly JM, Danberry TL, Augustine-Rauch KA. Development of a zebrafish embryo teratogenicity assay and quantitative prediction model. *Birth Defects Res. B Dev. Reprod. Toxicol. 89, 66–77. 2010.*

Bravatà V, Cammarata FP, Forte GI, Minafra L. "Omics" of HER2-positive breast cancer. *OMICS. 2013;17:119–129.*

Bravatà V, Stefano A, Cammarata FP, Minafra L, Russo G, Nicolosi S, Pulizzi S, Gelfi C, Gilardi MC, Messa C. Genotyping analysis and ^{18}FDG uptake in breast cancer patients: a preliminary research. *J Exp Clin Cancer Res. 2013 Apr 30;32(1):23*.

Brunner S, TŐkÉs T, SzabÓ ER, Polanek R, SzabÓ IZ, Reisz Z, GubÁn BK, SzijÁrtÓ AL, Brand M, Hans S, Karsch L, Lessmann E, Pawelke J, SchÜrer M, Beyreuther E, HideghÉty K. Dose-dependent Changes After Proton and Photon Irradiation in a Zebrafish Model. *Anticancer Res. 2020 Nov;40(11):6123-6135*.

Bump EA, Malaker K, editors. Radioprotectors: Chemical, Biological and Clinical Perspective. *Boca Raton, FL: CRC Press; 1998. pp. 53–109.*

Burgio E, Piscitelli P, Migliore L. Ionizing Radiation and Human Health: Reviewing Models of Exposure and Mechanisms of Cellular Damage. An Epigenetic Perspective. *Int J Environ Res Public Health. 2018 Sep 10;15(9):1971*.

Cai L, Lin C, Yang N, Huang Z, Miao S, Chen X, Pan J, Rao P, Liu S. Preparation and characterization of nanoparticles made from Co-incubation of SOD and glucose. *Nanomaterials. 2017;7(12)*.

Calabrese V, Cornelius C, Trovato-Salinaro A, Cambria MT, Locascio MS, Di Rienzo L, Condorelli DF, Mancuso C, De Lorenzo A, Calabrese EJ. The Hormetic Role of Dietary Antioxidants in Free Radical-Related Diseases. *Curr. Pharm. Des. 16 (2010) 877–883*.

Calvaruso M, Pucci G, Musso R, Bravatà V, Cammarata FP, Russo G, Forte GI, Minafra L. Nutraceutical Compounds as Sensitizers for Cancer Treatment in Radiation Therapy. *Int J Mol Sci. 2019 Oct 23;20(21):5267*.

Chang WJ and Hwang PP. Development of zebrafish epidermis. *Birth Defects Res C Embryo Today. 2011 Sep;93(3):205-14*.

Chen CC, Hsieh MS, Hsuuw YD, Huang FJ, Chan WH. Hazardous effects of curcumin on mouse embryonic development through a mitochondria-dependent apoptotic signaling pathway. *International Journal of Molecular Sciences. 2010;11(8):2839–2855*.

Chen J. Impaired cardiovascular function caused by different stressors elicits a common pathological and transcriptional response in zebrafish embryos. *Comparative Study Zebrafish. 2013 Sep;10(3):389-400*.

Chen WF, Deng SL, Zhou B, Yang L, Liu ZL. Curcumin and its analogues as potent inhibitors of low density lipoprotein oxidation: H-atom abstraction from the phenolic groups and possible involvement of the 4-hydroxy-3-methoxyphenyl groups. *Free Radic. Biol. Med. 2006;40:526–535*.

Chen X, Li Y, Yao T, Jia R. Benefits of Zebrafish Xenograft Models in Cancer Research. *Front Cell Dev Biol. 2021 Feb 11;9:616551*.

Chen Y, Lu Y, Lee RJ, Xiang G. Nano Encapsulated Curcumin: And Its Potential for Biomedical Applications. *Int J Nanomedicine. 2020 May 1;15:3099-3120*.

Chen YH, Yang ZS, Wen CC, Chang YS, Wang BC, Hsiao CA, Shih TL. Evaluation of the structure-activity relationship of flavonoids as antioxidants and toxicants of zebrafish larvae. *Food Chemistry. 2012;134(2):717–724*.

Chendil D, Ranga RS, Meigooni D, Sathishkumar S, Ahmed MM. Curcumin confers radiosensitizing effect in prostate cancer cell line PC-3. *Oncogene. 2004;23:1599–607*.

Citrin D, Cotrim AP, Hyodo F, Baum BJ, Krishna MC, and Mitchell JB. Radioprotectors and Mitigators of Radiation-Induced Normal Tissue Injury. *Oncologist. 2010 Apr; 15(4): 360–371*.

Citrin DE, Mitchell JB. Mechanisms of Normal Tissue Injury From Irradiation. *Semin Radiat Oncol. 2017 Oct;27(4):316-324*.

Costa B, Ferreira S, Póvoa V, Cardoso MJ, Vieira S, Stroom J, Fidalgo P, Rio-Tinto R, Figueiredo N, Parés O, Greco C, Ferreira MG, Fior R. Developments in zebrafish avatars as radiotherapy sensitivity reporters - towards personalized medicine. *EBioMedicine. 2020 Jan;51:102578*.

Daroczi B, Kari G, McAleer MF, Wolf JC, Rodeck U, Dicker AP. *In vivo* radioprotection by the fullerene nanoparticle DF-1 as assessed in a zebrafish model. *Clin Cancer Res. 2006 Dec 1;12(23):7086-91*.

Desouky O, Zhou G. Biophysical and radiobiological aspects of heavy charged particles. *Journal of Taibah University for Science, Volume 10, Issue 2, March 2016, Pages 187-194*.

Donmez G, Outeiro TF. SIRT1 and SIRT2: emerging targets in neurodegeneration. *EMBO Mol Med. 2013 Mar;5(3):344-52*.

Dulbecco P and Savarino V. Therapeutic potential of curcumin in digestive diseases. *World J. Gastroenterol., vol. 19, no. 48, pp. 9256–9270, 2013*.

Ellis AE, Stapleton KJ, Hastings TS. The humoral immune response of rainbow trout (*Salmo gairdneri*) immunised by various regimes and preparations of *Aeromonas salmonicida* antigens. *Vet Immunol Immunopathol. 1988 Sep;19(2):153-64*.

Forkasiewicz A, Dorociak M, Stach K, Szelachowski P, Tabola R, Augoff K. The usefulness of lactate dehydrogenase measurements in current oncological practice. *Cell Mol Biol Lett. 2020 Jun 9;25:35*.

Forte GI, Minafra L, Bravatà V, Cammarata FP, Lamia D, Pisciotta P, Cirrone GAP, Cuttone G, Gilardi MC, Russo G. Radiogenomics. The utility in patient selection. *Transl. Cancer Res. 2017, 6 (Suppl. 5), S852–S874*.

Gan L, Guo M, Si J, Zhang J, Liu Z, Zhao J, Wang F, Yan J, Li H, Zhang H. Protective effects of phenformin on zebrafish embryonic neurodevelopmental toxicity induced by X-ray radiation. *Artif. Cells Nanomed. Biotechnol. 2019, 47, 4202–4210*.

Geiger GA, Parker SE, Beothy AP, Tucker JA, Mullins MC, Kao GD. Zebrafish as a "Biosensor"? Effects of Ionizing Radiation and Amifostine on Embryonic Viability and Development. *Cancer Res 2006; 66: 8172-81*.

Goel A, Kunnumakkara AB, Aggarwal BB. Curcumin as "Curecumin": From kitchen to clinic. *Biochem. Pharm. 2008;75:787–809*.

Goodhead DT. Energy deposition stochastics and track structure: What about the target? *Radiat. Prot. Dosimetry. 2006;122:3–15*.

Greer EL and Brunet A. FOXO transcription factors at the interface between longevity and tumor suppression. *Oncogene. 2005 Nov 14;24(50):7410-25*.

Groves MD, Maor MH, Meyers C, Kyritsis AP, Jaeckle KA, Yung WK, Sawaya RE, Hess K, Bruner JM, Peterson P, and Levin VA. A phase II trial of high-dose bromodeoxyuridine with accelerated fractionation radiotherapy followed by procarbazine, lomustine, and vincristine for glioblastoma multiforme. *Int. J. Radiat. Oncol. Biol. Phys. 1999;45:127–135*.

Gu L, Chiang KY, Zhu N, Findley HW. and Zhou M. Contribution of STAT3 to the activation of survivin by GM-CSF in CD34+ cell lines. *(2007). Exp Hematol 35:957–966*.

Gu Q, Wang D, Cui C, Gao Y, Xia G, Cui X. Effects of radiation on wound healing. *J Environ Pathol Toxicol Oncol 1998;17:117–23*.

Hall EJ and Giaccia AJ. Radiobiology for the Radiologist. *(2006). 6th Edition, Lippincott Williams and Wilkins, Philadelphia*.

Hall EJ, Withers HR, Geraci JP, Meyn RE, Rasey J, Todd P, Sheline GE. Radiobiological intercomparisons of fast neutron beams used for therapy in Japan and the United States. *Int J Radiat Oncol Biol Phys. 1979 Feb;5(2):227-33*.

Horzmann KA and Freeman JL. Making Waves: New Developments in Toxicology With the Zebrafish. *Toxicol Sci. 2018 May 1;163(1):5-12*.

Howe K, Clark MD et al. The zebrafish reference genome sequence and its relationship to the human genome. *Nature. 2013 Apr 25;496(7446):498-503*.

Hu M, Hu N, Ding D, Zhao W, Feng Y, Zhang H, Li G, Wang Y. Developmental toxicity and oxidative stress induced by gamma irradiation in zebrafish embryos. *Radiat Environ Biophys. 2016 Nov;55(4):441-450*.

Hwang M, Yong C, Moretti L, Lu B. Zebrafish as a model system to screen radiation modifiers. *Curr. Genom. 2007;8:360–369.*

INTERNATIONAL ATOMIC ENERGY AGENCY, Absorbed Dose Determination in External Beam Radiotherapy. *Technical Reports Series No. 398, IAEA, Vienna (2000).*

Jäger R, Lowery RP, Calvanese AV, Joy JM, Purpura M, and Wilson JM. Comparative absorption of curcumin formulations. *Nutr J. 2014; 13: 11.*

Jagetia GC, Rajanikant GK. Curcumin Stimulates the Antioxidant Mechanisms in Mouse Skin Exposed to Fractionated γ-Irradiation. *Antioxidants (Basel). 2015 Jan 13;4(1):25-41.*

Jheng-Yu WU, Chin-Yi LIN, Tien-Wei LIN, Chuian-Fu KEN, and Yu-Der WEN. Curcumin Affects Development of Zebrafish Embryo. *Biol. Pharm. Bull. 30(7) 1336-1339. 2007.*

Kari G, Rodeck U and Dicker AP. Zebrafish: An Emerging Model System for Human Disease and Drug Discovery. *Clin Pharmacol Ther. 2007.*

Kim W, Kang J, Lee S, Youn B. Effects of traditional oriental medicines as anti-cytotoxic agents in radiotherapy. *Oncol Lett. 2017 Jun;13(6):4593-4601.*

Kimmel CB, Ballard WW, Kimmel SR, Ullmann B, Schilling TF. Stages of embryonic development of the zebrafish. *Dev Dyn. 1995 Jul;203(3):253-310.*

Lam SH, Chua HL, Gong Z, Wen Z, Lam TJ, Sin YM. Morphological transformation of the thymus in developing zebrafish. *Dev Dyn 2002;225:87–94.*

Li C, Shi L, Chen D, Ren A, Gao T, Zhao M. Functional analysis of the role of glutathione peroxidase (GPx) in the ROS signaling pathway, hyphal branching and the regulation of ganoderic acid biosynthesis in Ganoderma lucidum. *Fungal Genet Biol. 2015 Sep;82:168-80.*

Li J, Zhang Y, Liu K, He Q, Sun C, Han J, Han L, Tian Q. Xiaoaiping Induces Developmental Toxicity in Zebrafish Embryos Through Activation of ER Stress, Apoptosis and the Wnt Pathway. *Front Pharmacol. 2018 Nov 6;9:1250.*

Li X, Zha X, Wang Y, et al. Toxic effects and foundation of proton radiation on the early-life stage of zebrafish development. *Chemosphere. 2018;200:302–312.*

Lin SR, Chang CH, Hsu CF, Tsai MJ, Cheng H, Leong MK, Sung PJ, Chen JC, and Weng CF. Natural compounds as potential adjuvants to cancer therapy: Preclinical evidence. *Br J Pharmacol. 2020 Mar; 177(6): 1409–1423*.

Lu G, Guo M, Si J, Zhang J, Liu Z, Zhao J, Wang F, Yan J, Li H, Zhang H. Protective effects of phenformin on zebrafish embryonic neurodevelopmental toxicity induced by X-ray radiation. *Artif Cells Nanomed Biotechnol. 2019 Dec;47(1):4202-4210*.

Lühr A, von Neubeck C, Helmbrecht S, Baumann M, Enghardt W, Krause M. Modeling *in vivo* relative biological effectiveness in particle therapy for clinically relevant endpoints. *Acta Oncol. 2017 Nov;56(11):1392-1398*.

Lyng FM, O'Reilly S, Cottell DC, Seymour CB, Mothersill C. Persistent expression of morphological abnormalities in the distant progeny of irradiated cells. *Radiat. Environ. Biophys. 1996;35:273–283*.

MacRae CA, Peterson RT. Zebrafish as tools for drug discovery. *Nat Rev Drug Discov. 2015 Oct;14(10):721-31*.

Marín A, Martín M, Liñán O, Alvarenga F, López M, Fernández L, Büchser D, Cerezo L. Bystander effects and radiotherapy. *Rep Pract Oncol Radiother. 2014 Aug 28;20(1):12-21*.

McAleer MF, Davidson C, Davidson WR, Yentzer B, Farber SA, Rodeck U, Dicker AP. Novel use of zebrafish as a vertebrate model to screen radiation protectors and sensitizers. Int J Radiat Oncol Biol Phys 2005; 61: 10-13.

McBride WH, Schaue D. Radiation-induced tissue damage and response. *J Pathol. 2020 Apr;250(5):647-655*.

McCollum CW, Ducharme NA, Bondesson M and Gustafsson JA. Developmental toxicity screening in zebrafish. *(2011). Birth Defects Res. part C Embryo Today 93(2): 67-114*.

Meng H, Terado T, Kimura H. Apoptosis induced by X-rays and chemical agents in murine fibroblastic cell lines with a defect in repair of DNA double-strand breaks. *Int J Radiat Biol. 1998 May;73(5):503-10*.

Meyer DN, Baker BB, Baker TR. Ancestral TCDD Exposure Induces Multigenerational Histologic and Transcriptomic Alterations in Gonads of Male Zebrafish. *Toxicol Sci. 2018 Aug 1;164(2):603-612*.

Miao H, Hu N, Ding D, Zhao W, Feng Y, Zhang H, Li G, and Wang Y. Developmental toxicity and oxidative stress induced by gamma irradiation in zebrafish embryos. *Radiation and Environmental Biophysics volume 55, pages441–450 (2016)*.

Minafra L, Porcino N, Bravatà V, Gaglio D, Bonanomi M, Amore E, Cammarata FP, Russo G, Militello C, Savoca G, Baglio M, Abbate B, Iacoviello G, Evangelista G, Gilardi MC, Bondì ML, Forte GI. Radiosensitizing effect of curcumin-loaded lipid nanoparticles in breast cancer cells. *Sci Rep. 2019 Jul 31;9(1):11134*.

Montay-Gruel P, Meziani L, Yakkala C, Vozenin MC. Expanding the therapeutic index of radiation therapy by normal tissue protection. *Br J Radiol. 2019 Jan;92(1093):20180008*.

Moore S, Stanley FK, Goodarzi AA. The repair of environmentally relevant DNA double strand breaks caused by high linear energy transfer irradiation--no simple task. *DNA Repair (Amst). 2014 May;17:64-73*.

Mothersill C, Seymour C. Low-dose radiation effects: Experimental hematology and the changing paradigm. *Exp. Hematol. 2003;31:437–445*.

Murgia D, Angellotti G, Conigliaro A, Carfi Pavia F, D'Agostino F, Contardi M, Mauceri R, Alessandro R, Campisi G, De Caro V. Development of a Multifunctional Bioerodible Nanocomposite Containing Metronidazole and Curcumin to Apply on L-PRF Clot to Promote Tissue Regeneration in Dentistry. *Biomedicines. 2020 Oct 16;8(10):425*.

Najafi M, Motevaseli E, Shirazi A, Geraily G, Rezaeyan A, Norouzi F, Rezapoor S, Abdollahi H. Mechanisms of inflammatory responses to radiation and normal tissues toxicity: Clinical implications. *Int. J. Radiat. Biol. 2018;94:335–356*.

Nelson KM, Dahlin JL, Bisson J, Graham J, Pauli GF, Walters MA. The Essential Medicinal Chemistry of Curcumin. *J Med Chem. 2017 Mar 9;60(5):1620-1637*.

Nho RS, Hergert P. FoxO3a and disease progression. *World J Biol Chem. 2014 Aug 26;5(3):346-54*.

Oyemitan IA, Elusiyan CA, Onifade AO, Akanmu MA, Oyedeji AO, McDonald AG. Neuropharmacological profile and chemical analysis of fresh

rhizome essential oil of Curcuma longa (turmeric) cultivated in Southwest Nigeria. *Toxicology Reports. 2017;4:391–398*.

Padilla S, Hunter DL, Padnos B, Frady S, MacPhail RC. Assessing locomotor activity in larval zebrafish: Influence of extrinsic and intrinsic variables. *Neurotoxicol. Teratol. 33, 624–630. 2011*.

Paganetti H, Niemierko A, Ancukiewicz M, Gerweck LE, Goitein M, Loeffler JS, Suit HD. *Relative biological effectiveness* (RBE) values for proton beam therapy. *Int. J. Radiat. Oncol. Biol. Phys*. 2002;53:407–421.

Paganetti H. *Relative biological effectiveness* (RBE) values for proton beam therapy. Variations as a function of biological endpoint, dose, and linear energy transfer. *Phys. Med. Biol. 2014;59:R419–R472*.

Paramasivam M, Poi R, Banerjee H, Bandyopadhyay A. High performance thin layer chromatographic method for quantitative determination of curcuminoids in *Curcuma longa* germplasm. *Food Chem. 2009;113:640–644*.

Perlman RL. Mouse models of human disease: An evolutionary perspective. *Evol Med Public Health. 2016 May 21;2016(1):170-6.*

Prasanna PG, Stone HB, Wong RS, Capala J, Bernhard EJ, Vikram B, Coleman CN. Normal tissue protection for improving radiotherapy: Where are the Gaps? *Transl Cancer Res. 2012 Jun;1(1):35-48.*

Pucci G, Forte GI, Cavalieri V. Evaluation of Epigenetic and Radiomodifying Effects during Radiotherapy Treatments in Zebrafish. *Int J Mol Sci. 2021 Aug 22;22(16):9053*.

Rajagopal RE, Balasubramanian M, Kalyanaraman S. Raw turmeric and pure curcumin: a comparison of embryonic cytotoxicity in zebrafish. *IJBCP International Journal of Basic & Clinical Pharmacology. 2017;6:2020–2026.*

Rawson DM, Zhang T, Kalicharan D, Jongebloed WL. *Aquacult Res. 2000;31:325–336.*

Razaghi B, Steele SL, Prykhozhij SV, Stoyek MR, Hill JA, Cooper MD, McDonald L, Lin W, Daugaard M, Crapoulet N, Chacko S, Lewis SM, Scott IC, Sorensen PHB, Berman JN. hace1 Influences zebrafish cardiac development via ROS-dependent mechanisms. *Dev Dyn. 2018 Feb;247(2):289-303*.

Ruby AJ, Kuttan G, Babu KD, Rajasekharan KN, Kuttan R. Anti-tumour and antioxidant activity of natural curcuminoids. *Cancer Lett. 1995 Jul 20;94(1):79-83*.

Saager M, Peschke P, Welzel T, Huang L, Brons S, Grün R, Scholz M, Debus J, Karger CP. Late normal tissue response in the rat spinal cord after carbon ion irradiation. *Radiat Oncol. 2018 Jan 11;13(1):5*.

Sachett A, Benvenutti R, Reis CG, Gallas-Lopes M, Bastos LM, Aguiar GPS, Herrmann AP, Oliveira JV, Siebel AM, Piato A. Micronized curcumin causes hyperlocomotion in zebrafish larvae. *Neurochem Res. 2022 Aug;47(8):2307-2316*.

Saint-Amant L and Drapeau P. Time Course of the Development of Motor Behaviors in the Zebrafish Embryo. *(1998) Journal of Neurobiology, 37, 622-632*.

Salehi B, Calina D, Docea AO, Koirala N, Aryal S, Lombardo D, Pasqua L, Taheri Y, Marina Salgado Castillo C, Martorell M, Martins N, Iriti M, Suleria HAR, Sharifi-Rad J. Curcumin's Nanomedicine Formulations for Therapeutic Application in Neurological Diseases. *J Clin Med. 2020 Feb 5;9(2):430*.

Samaee SM, Rabbani S, Jovanović B, Mohajeri-Tehrani MR, Haghpanah V. Efficacy of the hatching event in assessing the embryo toxicity of the nano-sized TiO2 particles in zebrafish: A comparison between two different classes of hatching-derived variables. *Ecotoxicol Environ Saf. 2015 Jun;116:121-8*.

Sato K, Tsuchida S, Tamai K, Ryoho GTK. Anti-cancer drug resistance and glutathione S-transferases. *1989 Mar;16(3 Pt 2):592-8*.

Savoca G, Calvaruso M, Minafra L, Bravatà V, Cammarata FP, Iacoviello G, Abbate B, Evangelista G, Spada M, Forte GI, Russo G. *Local Disease-Free Survival Rate* (LSR) Application to Personalize Radiation Therapy Treatments in Breast Cancer Models. *J Pers Med. 2020 Oct 17;10(4):177*.

Selderslaghs IWT, Van Rompay AR, De Coen W, Witters HE. Development of a screening assay to identify teratogenic and embryotoxic chemicals using the zebrafish embryo. *Reprod. Toxicol. 28, 308–320. 2009*.

Shabeeb D, Musa AE, Ali HSA, Najafi M. Curcumin Protects Against Radiotherapy-Induced Oxidative Injury to the Skin. *Drug Des. Dev. Ther. 2020;14:3159–3163*.

Shiau RJ, Shih PC, Wen YD. Effect of silymarin on curcumin-induced mortality in zebrafish (*Danio rerio*) embryos and larvae. *Indian J Exp Biol. 2011 Jul;49(7):491-7.*

Si J, Zhou R, Zhao B, Xie Y, Gan L, Zhang J, Wang Y, Zhou X, Ren X, Zhang H. Effects of ionizing radiation and HLY78 on the zebrafish embryonic developmental toxicity. *Toxicology. 2019;411:143–153.*

Sipes NS, Padilla S, Knudsen TB. Zebrafish: as an integrative model for twenty-first century toxicity testing. *Birth Defects Res C Embryo Today. 2011 Sep;93(3):256-67.*

Somasagara RR, Leung TC. Methods Mol Biol. Zebrafish Xenograft Model to Study Human Cancer. 2022;2413:45-53.

Srinivasan M, Ram Sudheer A, Rajasekaran KN, Menon Venugopal P. Effect of curcumin analog on gamma-radiation-induced cellular changes in primary culture of isolated rat hepatocytes in vitro. *Chem Biol Interact. 2008 Oct 22;176(1):1-8.*

Srivastava M, Chandra D, Kale RK. Modulation of radiation-induced changes in the xanthine oxidoreductase system in the livers of mice by its inhibitors. *Radiat Res. 2002 Mar;157(3):290-7.*

Steel GG. Basic Clinical Radiobiology. *First published in Great Britain, 1993.*

Stehr CM, Linbo TL, Incardona JP and Scholz NL. The developmental neurotoxicity of fipronil: notochord degeneration and locomotor defects in zebrafish embryos and larvae. *(2006) Toxicological Sciences 92 (1): 270–278.*

Suhe D, Lyu X, Yuan S, Wang S, Li W, Chen Z, Yu H, Li F, Jiang Q. Oxidative stress: A critical hint in ionizing radiation induced pyroptosis. *Radiation Medicine and Protection. Volume 1, Issue 4, December 2020, Pages 179-185.*

Szabó ER, Brand M, Hans S, Hideghéty K, Karsch L, Lessmann E, Pawelke J, Schürer M, Beyreuther E. Radiobiological effects and proton RBE determined by wildtype zebrafish embryos. *PLoS One. 2018 Nov 8;13(11):e0206879.*

Szabó ER, Plangár I, Tőkés T, Mán I, Polanek R, Kovács R, Fekete G, Szabó Z, Csenki Z, Baska F, Hideghéty K. l-Alpha Glycerylphosphorylcholine as a

Potential Radioprotective Agent in Zebrafish Embryo Model. *Zebrafish. 2016 Dec;13(6):481-488*.

Tammineni P, Anugula C, Mohammed F, Anjaneyulu M, Larner AC. and Sepuri NB. (2013). The import of the transcription factor STAT3 into mitochondria depends on GRIM-19, a component of the electron transport chain. *J Biol Chem 288:4723–4732*.

Tang H, Cai L, He X, Niu Z, Huang H, Hu W, Bian H, Huang H. Radiation-induced bystander effect and its clinical implications. *Front Oncol. 2023 Apr 5;13:1124412*.

Tatner MF. Natural changes in the immune system of fish. In: Iwama GK, Nakanishi T, editors. The fish immune system: organism, pathogen and environment. *London: Academic Press; 1996. p. 255–87*.

Tew KD. Glutathione-associated enzymes in anticancer drug resistance. *Cancer Res. 1994 Aug 15;54(16):4313-20*.

Tommasino F and Durante M. Proton radiobiology. *Cancers (Basel). 2015 Feb 12;7(1):353-81*.

Trede NS, Langenau DM, Traver D, Look AT, Zon LI. The use of zebrafish to understand immunity. *Immunity. 2004;20:367–379*.

Tubin S, Fossati P, Mock U, Lütgendorf-Caucig C, Flechl B, Pelak M, Georg P, Fussl C, Carlino A, Stock M, Hug E. Proton or Carbon Ion Therapy for Skull Base Chordoma: Rationale and First Analysis of a Mono-Institutional Experience. *Cancers (Basel). 2023 Mar 31;15(7):2093*.

Urano M, Verhey LJ, Goitein M, Tepper JE, Suit HD, Mendiondo O, Gragoudas ES, Koehler A. Relative biological effectiveness of modulated proton beams in various murine tissues. *Int J Radiat Oncol Biol Phys. 1984 Apr;10(4):509-14*.

Uzawa A, Ando K, Furusawa Y, Kagiya G, Fuji H, Hata M, Sakae T, Terunuma T, Scholz M, Ritter S, Peschke P. Biological intercomparison using gut crypt survivals for proton and carbon-ion beams. *J Radiat Res. 2007;48 Suppl A:A75-80*.

Valvona CJ, Fillmore HL, Nunn PB, Pilkington GJ. The Regulation and Function of Lactate Dehydrogenase A: Therapeutic Potential in Brain Tumor. *Brain Pathol. 2016 Jan;26(1):3-17*.

Vasiliki Z, Vasiliki G, Pericles T, Athanasios PK, Alexiou GA. Radiosensitization and Radioprotection by Curcumin in Glioblastoma and Other Cancers. *Biomedicines. 2022 Jan 28;10(2):312*.

Vettraino M, Manerba M, Govoni M, Di Stefano G. Galloflavin suppresses lactate dehydrogenase activity and causes MYC downregulation in Burkitt lymphoma cells through NAD/NADH-dependent inhibition of sirtuin-1. *Anticancer Drugs. 2013 Sep;24(8):862-70*.

Vogel AM, Weinstein BM. Studying vascular development in the zebrafish. *Trends Cardiovasc. Med. 2000;10:352–360*.

Völkel P, Dupret B, Le Bourhis X, Angrand PO. The zebrafish model in oncology. *Med Sci (Paris). 2018 Apr;34(4):345-353.*

Wabik A, Jones PH. Switching roles: the functional plasticity of adult tissue stem cells. *EMBO J 2015; 34 : 1164–1179*.

Wakeford R. The cancer epidemiology of radiation. *Oncogene. 2004;23:6404–6428*.

Wang X, Zhang H, Gao Y, and Zhang W. Characterization of Cu/Zn-SOD enzyme activities and gene expression in soybean under low nitrogen stress. *J Sci Food Agric. 2016;96(8): 2692–2697*.

Wan-Mohtar W, Ilham Z, Jamaludin AA, and Rowan N. Use of Zebrafish Embryo Assay to Evaluate Toxicity and Safety of Bioreactor-Grown Exopolysaccharides and Endopolysaccharides from European Ganoderma applanatum Mycelium for Future Aquaculture Applications. *Int J Mol Sci. 2021 Feb; 22(4): 1675*.

Warkentin B, Stavrev P, Stavreva N, Field C, Fallone BG. A TCP-NTCP estimation module using DVHs and known radiobiological models and parameter sets. *J Appl Clin Med Phys. 2004 Winter;5(1):50-63*.

Wasundara Fernandoa HP, Rupasinghead V, Hoskinabc DW. Dietary phytochemicals with anti-oxidant and pro-oxidant activities: A double-edged sword in relation to adjuvant chemotherapy and radiotherapy? *Cancer Letters Volume 452, 28 June 2019, Pages 168-177*.

Wegrzyn J, Potla R, Chwae YJ, Sepuri NB, Zhang Q, Koeck T, Derecka M, Szczepanek K, Szelag M, et al. (2009). Function of mitochondrial Stat3 in cellular respiration. *Science 323:793–797*.

Westerfield M. (2007) The Zebrafish Book 5th edition – A guide for the laboratory use of zebrafish (*Danio rerio*). Univ. of Oregon Press.

Wu L, Cole A, Du W. Immune-DDR crosstalk in pre-leukemia stem cells. *Oncotarget. 2017 Sep 19;8(47):81731-81732.*

Xia Q, Wei L, Zhang Y, Kong H, Shi Y, Wang X, Chen X, Han L, Liu K. Psoralen Induces Developmental Toxicity in Zebrafish Embryos/Larvae Through Oxidative Stress, Apoptosis, and Energy Metabolism Disorder. *Front Pharmacol. 2018 Dec 18;9:1457.*

Yallapu MM, Khan S, Maher DM, Ebeling MC, Sundram V, Chauhan N, Ganju A, Balakrishna S, Gupta BK, Zafar N, Jaggi M, and Chauhan SC. Anti-cancer activity of curcumin loaded nanoparticles in prostate cancer. *Biomaterials, vol. 35, no. 30, pp. 8635–8648, 2014.*

Yorke ED, Jackson A, Rosenzweig KE, Merrick SA, Gabrys D, Venkatraman ES, Burman CM, Leibel SA, Ling CC. Dose-volume factors contributing to the incidence of radiation pneumonitis in non-small-cell lung cancer patients treated with three-dimensional conformal radiation therapy. *Int J Radiat Oncol Biol Phys. 2002;54:329–339.*

Yu H, Pardoll D, Jove R. STATs in cancer inflammation and immunity: a leading role for STAT3. *Nat Rev Cancer. 2009 Nov;9(11):798-809.*

Yuqing W, Nartiss Y, Steipe B, McQuibban GA, Kim PK. ROS-induced mitochondrial depolarization initiates PARK2/PARKIN-dependent mitochondrial degradation by autophagy. *Autophagy. 2012 Oct;8(10):1462-76.*

Zhou R, Zhang H, Wang Z, et al. The developmental toxicity and apoptosis in zebrafish eyes induced by carbon-ion irradiation. *Life Sci. 2015;139:114–122.*

Zoi V, Galani V, Tsekeris P, Kyritsis AP, Alexiou GA. Radiosensitization and Radioprotection by Curcumin in Glioblastoma and Other Cancers. *Biomedicines. 2022 Jan 28;10(2):312.*